Investigation of compensatory autophagy and T cell senescence during proteasome dysfunction

（プロテアソーム機能低下に伴う代償的オートファジー及びT 細胞老化に関する研究）

荒田　義之

Investigation of compensatory autophagy and T cell senescence during proteasome dysfunction

（プロテアソーム機能低下に伴う代償的オートファジー及びT 細胞老化に関する研究）

荒田　義之

論文の内容の要旨

論文題目　プロテアソーム機能低下に伴う代償的オートファジー及び T 細胞老化に関する研究

氏名　荒田　義之

プロテアソームは細胞内タンパク質分解を介して様々な生命現象に関与している。そのため、プロテアソーム機能の低下は、生体に広範な異常を来し、近年では特に老化との関連が注目されている。したがって、プロテアソーム機能低下時に生体がどのように応答をし、細胞・個体老化に至るのかの理解は、老化あるいは加齢に伴い発症率の上昇する自己免疫疾患等の予防や治療にむけて重要になりうる。本研究ではプロテアソーム機能低下時に起こる生命現象について、Part A) プロテアソーム機能低下に応じて代償的に誘導されるオートファジー活性化機構 Part B) T 細胞老化に伴うプロテアソーム機能低下に着目して研究を行なった。

Part A: プロテアソーム機能低下時の代償的オートファジー誘導機構

プロテアソームの形成シャペロン p28 と結合する因子を質量分析法により網羅的に解析したところ、プロテアソーム阻害剤処置条件下において FAM48A が結合因子の 1 つとして同定された。FAM48A は今までプロテアソームとの関連は報告されていなかったが、オートファジーを制御することが知られる因子であった。主要な細胞内タンパク質分解系であるユビキチン・プロテアソームシステムとオートファジーは協調して働き、プロテアソーム機能低下時にオートファジーが代償的に誘導され、細胞の機能維持にはたらくことが知られる。しかしながら、その詳細なメカニズムは不明であった。そこで FAM48A が代償的オートファジーを制御する可能性を考え解析を行った。

プロテアソーム機能低下時に誘導される代償的オートファジー誘導に FAM48A が関与するか調べるために FAM48A のノックダウンを行なった。オートファジー誘導のマーカーである LC3-II の蓄積及び LC3 のドット状構造の形成をそれぞれウエスタンブロット法及び免疫染色法で評価したところ、FAM48A のノックダウンによりプロテアソームを阻害した細胞における

オートファジー誘導が顕著に抑制された（図 1a, b）。このことから FAM48A はプロテアソーム機能低下時に誘導される代償的オートファジーを仲介することが示唆された。

FAM48A はオートファジーに必須の因子である Atg9 と結合することが知られる。Atg9 はトランスゴルジ網あるいはエンドソームを介したメンブレントラフィックによって脂質供給を行い、オートファジー誘導働く。Atg9 とそれぞれトランスゴルジ網マーカー及びリサイクリングエンドソームのマーカーである GM130 及び Rab11 との共局在を調べたところ、プロテアソーム阻害剤処置した細胞において Atg9 と GM130 あるいは Rab11 の共局在は FAM48A ノックダウンにより顕著に減少した。このことから FAM48A はプロテアソーム機能低下時に Atg9 のメンブレントラフィックを制御することが示唆された。

以上の結果から新規に同定したプロテアソーム結合因子 FAM48A がプロテアソーム機能低下時に Atg9 のメンブレントラフィック制御を介してオートファジーを代償的に誘導する分子メカニズムの一端が示された。

Part B: T 細胞老化に伴うプロテアソーム機能低下

プロテアソーム機能は老化の過程及び CD4 陽性 T 細胞依存的な免疫反応に深く関わることが知られている。しかしながら、CD4 陽性 T 細胞の老化とプロテアソーム機能の関連は未知であった。

まずプロテアソーム機能低下が CD4 陽性 T 細胞において老化を引き起こす可能性について検討した。T 細胞受容体（TCR）刺激した CD4 陽性 T 細胞をプロテアソーム阻害剤処置したところ、p21 発現上昇を伴った細胞増殖の低下及び細胞老化関連分泌形質（SASP）関連遺伝子の上昇がみられた。さらにプロテアソームの必須サブユニットの 1 つである Rpn13 を T 細胞特異的に欠損したマウスでは PD-1^{+} CD44^{High} CD4 陽性 T の増加が見られた。これらの特徴は老化 CD4 陽性 T 細胞が示す特徴と合致しており、プロテアソーム機能低下は CD4 陽性 T 細胞においても老化様の症状を促進することが示唆された。

一部の細胞腫では老化に伴いプロテアソームの量が減少することが知られており、本研究においては CD4 陽性 T 細胞におけるプロテアソームの量的制御機構を調べた。TCR 刺激した CD4 陽性 T 細胞において、すべてのプロテアソームサブユニットの遺伝子発現及びプロテアソーム活性の上昇がみられたことから、TCR 刺激依存的にプロテアソームを誘導す

る機構が認められた。また、阻害剤を用いた検討からこの発現誘導は TCR の下流の MEK、IKK、及びカルシニューリン依存的な経路を介することが示唆された。

CD4 陽性 T 細胞においてプロテアソーム機能が加齢に伴い減少しているか確認するためにプロテアソームサブユニット Rpn11 の C 末端に GFP を付加したノックインレポーターマウスを用いて検討を行なった。脾臓から分取した細胞をフローサイトメトリーにより解析したところ定常状態では CD4 陽性 T 細胞中の Rpn11-GFP 量の加齢に応じた減少はみられなかった。一方で TCR 刺激した CD4 陽性 T 細胞を調べたところ、加齢依存的にプロテアソーム発現誘導が減弱した細胞集団の増加がみられた（図 2）。各種 CD4T 細胞のサブポピュレーションごとのプロテアソーム誘導能を調べたところ、老齢マウスで増加することが知られる PD-1^{+} $CD44^{High}$ CD4 陽性 T 細胞において顕著にプロテアソーム誘導が減弱していた。

以上の結果からプロテアソームの発現誘導の減弱が CD4 陽性 T 細胞老化の特性の 1 つであることが示された。

【まとめ】

本研究において主要な細胞内タンパク質分解系であるプロテアソームとオートファジーを介在する新規因子として FAM48A を同定した。FAM48A はプロテアソーム機能阻害時に細胞内に蓄積することからプロテアソーム機能低下を感知するセンサーとしての役割をもち、Atg9 のメンブレントラフィックの制御を介して代償的オートファジー活性化に働くと考えられる。プロテアソーム機能低下時に蓄積した FAM48A が Atg9 の局在を制御する詳細な機構は未知であり、今後解明すべき課題である。

プロテアソームの発現量は細胞の種類や細胞の置かれる環境に応じて変化することが近年わかってきたが、その制御機構は未解明な部分が多い。本研究では TCR 刺激依存的にプロテアソーム発現量が増加すること、さらに加齢に伴いその発現誘導が減弱していくことが示され、T 細胞に特有のプロテアソーム発現制御機構が明らかとなった。老化 CD4 陽性 T 細胞は SASP 因子の分泌を介しマウスにおいて自己免疫疾患を引き起こすことが知られているが、本研究においてプロテアソーム機能低下は CD4 陽性 T 細胞における SASP 因子の発現亢進を引き起こすこと、及び老化 CD4 陽性 T 細胞において TCR 刺激に伴うプロテアソ

ーム機能上昇が抑制されることが明らかになった。そのため老化 CD4 陽性 T 細胞における
プロテアソーム誘導を抑制する機構は加齢性疾患の治療標的となることが期待される。

【図 1】

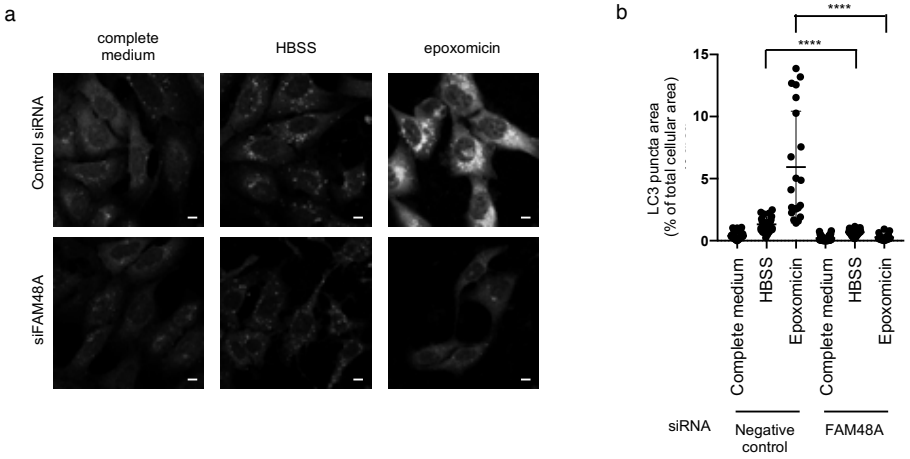

【図 2】

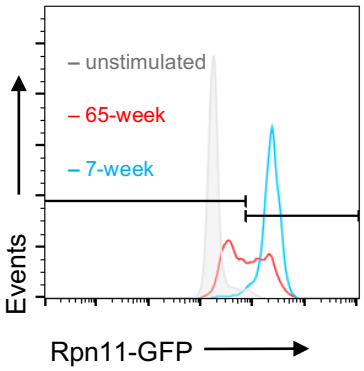

Part A: FAM48A mediates compensatory autophagy induced by proteasome impairment

Abstract

Maintaining protein homeostasis is central to cell survival. The ubiquitin–proteasome system and autophagy play pivotal roles in protein quality control through protein degradation. Activities of these degradative pathways are carefully orchestrated, and autophagy is upregulated during proteasome dysfunction for cellular homeostasis. However, the mechanism by which proteasome impairment induces compensatory autophagy has remained largely elusive. Here, we show that FAM48A mediates autophagy induction during proteasome inhibition. FAM48A is degraded by the proteasome and accumulates in cells by proteasome inhibition. Knockdown of FAM48A led to defective induction of autophagy during proteasome inhibition, accompanied by defective localization of Atg9 on recycling endosomes. Our results indicate that FAM48A is a kind of sensor that is required for compensatory autophagy induction upon proteasome impairment.

Introduction

The ubiquitin–proteasome system (UPS) and macroautophagy (hereafter referred to as autophagy) are the principal pathways for intracellular protein degradation. The 26S proteasome is an ATP-dependent protease complex responsible for the degradation of polyubiquitinated proteins in eukaryotic cells[1,2]. In autophagy, the autophagosome engulfs a portion of the cytoplasm and then fuses with the lysosome to degrade the sequestered content[3].

Protein homeostasis is maintained through regulation of the quality and capacity of protein translation, folding, and degradation in cells. Disturbance of protein homeostasis has deleterious effects including cancer, neurodegeneration, and aging[4–10]. The two major degradation systems, the UPS and autophagy, coordinately play pivotal roles in removing aberrant proteins to maintain protein homeostasis. As the activity of the proteasome declines, proteasome biogenesis is upregulated by activating the transcriptional cascade through Nrf1 and DDI2 to compensate for the reduced degradative capacity of the proteasome[11–13]. Besides an increase in de novo proteasome synthesis, autophagy is upregulated to compensate for the reduced degradative capacity of intracellular protein in response to proteasome impairment[14].

Several reports have suggested that this compensatory autophagy is induced by a stress response elicited during proteasome impairment. Mitochondrial ROS production and depletion of amino acids during proteasome dysfunction cause the activation of autophagy through sensing via AMPK and mTORC1, respectively[15–17]. Proteasome impairment also induces endoplasmic reticulum (ER) stress, which then

triggers transcriptional upregulation of autophagy-related genes[18–20]. We considered the possibility that a proteasomal substrate protein accumulates and could play a role in autophagy induction in response to proteasome impairment, analogous to Nrf1 in the induction of proteasome synthesis.

In this study, beginning with interactome analysis, we showed that proteasome impairment and compensatory autophagy activation are interconnected with FAM48A (also known as SUPT20H/p38IP), a newly identified proteasomal substrate. FAM48A is required for the localization of Atg9 to the recycling endosome and thus for autophagy induction upon proteasome inhibition.

Results

Identification of FAM48A as a proteasome-associated protein during proteasome inhibition

We expected that proteasome-associated proteins under proteasome impairment might play a compensatory role in proteasome dysfunction. To identify such proteins, HEK293T cells were transfected with Flag-tagged p28, a proteasome assembly chaperone, treated with the proteasome inhibitor MG132, and subjected to immunoprecipitation with anti-Flag antibody, followed by liquid chromatography coupled with tandem mass spectrometry (LC-MS/MS) [21]. In addition to proteasome subunits, we identified FAM48A, whose relevance to the proteasome was previously unknown (Figure 1a).

FAM48A is a multifunctional protein involved in autophagy, cell cycle regulation, ER stress response, and gastrulation. It executes these functions through interacting with proteins such as p38, Atg9, and the GCN5–SAGA complex[22–25]. Besides a nuclear localization signal (NLS) and PEST sequence in the N-terminal half, FAM48A has been shown to have a region that interacts with Atg9 (487–733 aa) (Figure 1b)[22,24].

Indeed, the proteasome subunit α6 was found to be co-immunoprecipitated with Flag-FAM48A in the presence of MG132 (Figure 1c). These results suggest that FAM48A is a novel proteasome associated protein during proteasome inhibition.

FAM48A is a proteasomal substrate.

As the amount of Flag-FAM48A was increased by MG132 treatment (Figure 1c), we next examined whether endogenous FAM48A also accumulates upon proteasome inhibition. For this purpose, we treated U2OS cells with epoxomicin, followed by the performance of immunoblot analysis. Endogenous FAM48A was accumulated in epoxomicin-treated cells (Figure 1d), while the expression of FAM48A mRNA did not increase in epoxomicin-treated cells (Figure 1e). These results suggest that FAM48A is mainly degraded by the proteasome.

FAM48A is required for autophagy induction triggered by proteasome dysfunction

It has been reported that impairment of the UPS induces compensatory autophagy[26]. On the other hand, FAM48A has been shown to regulate starvation-induced autophagy[22]. Since FAM48A accumulates upon proteasome inhibition, we speculated that it might be involved in compensatory autophagy triggered by proteasome inhibition.

To test this possibility, we monitored autophagosome formation by the immunohistochemical analysis of LC3 in U2OS cells. The number of LC3 punctate structures has been shown to correlate with the number of autophagosomes[27]. The cells were incubated in either complete medium, Hank's buffered salt solution (HBSS), or complete medium with epoxomicin and then stained with anti-LC3 antibody (Figure 2a). The ratio of the total area of LC3-positive puncta to the total cellular area was quantified (Figure 2b). Culture in amino-acid-deficient HBSS induced autophagosome formation, and knockdown of FAM48A significantly suppressed starvation-induced

autophagosome formation (Figure 2a and b), as reported in previous studies[22]. Treatment with epoxomicin induced massive LC3-positive puncta, as reported in previous studies[16]. However, when cells were transfected with an siRNA targeting FAM48A, the accumulation of LC3-positive puncta disappeared (Figure 2a and b). The effect of FAM48A knockdown was slight during amino acid starvation, compared with its effect on epoxomicin-induced autophagosome formation (Figure 2a and b). The knockdown efficiency of FAM48A in U2OS cells was confirmed by real-time PCR (Supporting Information Figure S1a).

To confirm this observation, the cell lysates under the above culture conditions were subjected to immunoblot analysis for LC3, in which an increase in the lipidation form LC3-II represents an increase in autophagosomes[27]. To assess autophagy flux, we also tested conditions with chloroquine. Chloroquine treatment led to an increase in LC3-II under culture conditions of either complete medium, HBSS, or epoxomicin (Figure 2c, lanes 1, 3, 5, 7, 9, and 11). In epoxomicin-treated cells, LC3-II accumulated more than in cells cultured in complete medium and HBSS (Figure 2c, lanes 1, 5, and 9), which is consistent with the results in Figure 2a and 2b. However, this accumulation was markedly suppressed by the knockdown of FAM48A (Figure 2c, lanes 9 and 10). The decrease of LC3-II in FAM48A-knockdown cells treated with epoxomicin was not due to enhancement of lysosomal degradation because chloroquine treatment did not cause the accumulation of LC3-II in FAM48A-knockdown cells treated with epoxomicin (Figure 2c, lanes 10 and 12). Since protein amounts of LC3 including both LC3-I and LC3-II decreased in FAM48A-knockdown cells, we

examined the expression of LC3 mRNA that is known to be induced during proteasome inhibition[28]. Although LC3 expression was downregulated in cells treated with FAM48A siRNA, LC3 mRNA was induced upon epoxomicin treatment regardless of transfection of FAM48A siRNA (Figure 2d). These results suggest that FAM48A plays a predominant role in autophagosome formation induced by proteasome dysfunction.

FAM48A regulates the localization of Atg9 on recycling endosomes during proteasome inhibition

Atg9 plays a crucial role in autophagosome formation through cycling between the trans-Golgi network (TGN) and cytoplasm including the endosomal system[29–31]. Since FAM48A interacts with Atg9 through its C-terminal region[22], we examined the possibility that FAM48A regulates compensatory autophagy through modulating the function of Atg9.

U2OS cells were transfected with FAM48A siRNA and stained with Atg9 and the TGN marker GM130. In cells cultured in complete medium and HBSS, Atg9 mainly localized to the TGN regardless of siRNA transfection. In cells treated with epoxomicin, Atg9 also localized to the TGN, but when FAM48A was knocked down, Atg9 was dispersed in the cytoplasm (Figure 3a and b).

It has been shown that Atg9 localizes to recycling endosomes (REs) as well as the Golgi apparatus[32]. To further confirm the regulation of Atg9 localization by FAM48A, we used COS-1 cells for visualizing endocytic trafficking pathways in more detail. In COS-1 cells, endocytic organelles are uniquely localized, and REs show

restricted localization within the ring-shaped structure of the Golgi complex[33]. Consistent with this report, the RE marker mKate2-Rab11 dispersed in the cytoplasm in U2OS cells, while mKate2-Rab11 localized within the GM130-positive ring-shaped structures (Supporting Information Figure S2a and b). Further, Atg9 also mainly localized in these ring-shaped structures in COS-1 cells (Supporting Information Figure S2c).

In addition, to avoid the possibility of off-target effects of siRNA, we used an additional FAM48A siRNA targeting a different sequence. The knockdown efficiency of FAM48A in COS-1 cells was confirmed by real-time PCR (Supporting Information Figure S1b). In COS-1 cells stably expressing Venus-Atg9 and the RE marker mKate2-Rab11, Atg9 co-localized to Rab11 under the conditions of complete medium and HBSS, and FAM48A siRNA transfection had no apparent effect on this co-localization (Figure 4a and b). On the other hand, the co-localization of Atg9 and Rab11 was diminished by the application of FAM48A siRNA during epoxomicin treatment (Figure 4a and b).

Next, to examine whether this diminished co-localization was caused by the reduction of Atg9 and/or RE or dispersion from REs, we quantified the cellular content of Venus-Atg9 and mKate2-Rab11 by flow cytometry. The median fluorescent intensity (MFI) of Venus-Atg9 was not decreased by epoxomicin treatment compared with that of cells cultured in either complete medium or HBSS (Figure 4c). In addition, the MFI of mKate2-Rab11 was not decreased (Figure 4d). These results suggest that the diminished co-localization of Atg9 and REs was due to defective trafficking of Atg9

between REs and cytoplasm, not due to a reduction of Atg9 or REs. These results suggest that FAM48A regulates the trafficking of Atg9 to REs during proteasome inhibition.

FAM48A is mainly localized to the nucleus during proteasome inhibition

Since it has been reported that FAM48A interacts with Atg9, we speculated that the intracellular dynamics of FAM48A might regulate Atg9 trafficking through direct binding between these two molecules. To test this, we examined the intracellular distribution of FAM48A using U2OS cells transiently expressing 3×Flag-FAM48A. FAM48A was localized mainly in the nucleus under complete medium- and HBSS-culture conditions, as reported in a previous study[24], and epoxomicin treatment did not alter the nuclear localization of FAM48A (Figure 5a). The nuclear localization of FAM48A was also confirmed by biochemical fractionation, followed by immunoblotting. FAM48A was accumulated predominantly in the nuclear fraction, not in the cytoplasmic fraction, during proteasome inhibition (Figure 5b). These results suggest that the regulation of Atg9 trafficking by FAM48A during proteasome inhibition did not occur through direct binding between Atg9 and FAM48A in the cytoplasm.

Discussion

In the present study, we identified FAM48A as a protein that interacts with the proteasome and regulates autophagy under proteasome impairment. FAM48A accumulated in cells during proteasome inhibition and contributed to the induction of autophagy and regulation of Atg9 localization. The localization of Atg9 in REs was significantly diminished during proteasome inhibition by the knockdown of FAM48A (Figure 3 and 4), along with the defective induction of autophagy (Figure 2). Atg9 cycles between the TGN and the endosomal system via vesicle trafficking, and a fraction of Atg9 transiently participates in the autophagic precursor structure, followed by autophagy induction [29,31,34]. More specifically, appropriate regulation of Atg9 trafficking via REs is indispensable for autophagosome formation[35], since Atg9–Atg2–Atg18 complex could supply phospholipid from membrane source[36,37], and REs serve as a membrane source of autophagosomes[30,34,38]. These results indicate that FAM48A is required for RE localization of Atg9 during proteasome inhibition, which is essential for compensatory autophagy induction.

The mechanism by which FAM48A regulates Atg9 trafficking during proteasome dysfunction also remains incompletely understood. We first speculated that the increased interaction between FAM48A and Atg9 elicits the autophagy machinery during proteasome inhibition, as observed in starving conditions in a previous study[22]. This idea, however, does not appear to explain the mechanism of autophagy induction during proteasome inhibition, since FAM48A accumulated in the nucleus, where Atg9 is absent (Figure 5b), and did not colocalize with Atg9 during proteasome inhibition

(Figure 5a). Another possibility is that FAM48A transcriptionally regulates genes that are involved in the trafficking of Atg9. It has been reported that FAM48A induces the expression of ER stress-responsive genes as a subunit of the transcriptional coactivator hSAGA complex[25], and FAM48A indeed localized primarily in the nucleus (Figure 5). Thus, the identification of genes whose expression under proteasome inhibition is dependent on FAM48A might aid in understanding the mechanism of the compensatory autophagy induction and cell survival under proteasome impairment.

Part B: Defective induction of the proteasome associated with T cell receptor signaling underlies T cell senescence

Abstract

The proteasome degradation machinery is essential for a variety of cellular processes including senescence and T cell immunity. Decreased proteasome activity is associated with the aging process; however, the regulation of the proteasome in $CD4^+$ T cells in relation to aging is unclear. Here, we show that defects in the induction of the proteasome in $CD4^+$ T cells upon T-cell receptor (TCR) stimulation underlie T cell senescence. Proteasome dysfunction promotes senescence-associated phenotypes, including defective proliferation, cytokine production, and increased levels of PD-1^+ $CD44^{High}$ $CD4^+$ T cells. Proteasome induction by TCR signaling via MEK-, IKK-, and calcineurin-dependent pathways is attenuated with age and decreased in PD-1^+ $CD44^{High}$ $CD4^+$ T cells, the proportion of which increases with age. Our results indicate that defective induction of the proteasome is a hallmark of $CD4^+$ T cell senescence.

Introduction

The 26S proteasome is a protease complex that functions in various biological processes by catalyzing the degradation of ubiquitin-tagged proteins. The expression and activity of the proteasome are closely associated with longevity and senescence[39–42]. Proteasomes are highly expressed in the longest living rodent, the naked mole rat[43]. High levels of proteasome expression are essential for the immortality and pluripotency of human embryonic stem cells[40]. Artificially increasing proteasome activity extends the lifespan of *Drosophila melanogaster* and *Caenorhabditis elegans*[40,42,44]. By contrast, proteasome dysfunction elicits senescence-like phenotypes including growth arrest and a shorter lifespan[45–47], which often occurs concomitant with autoinflammation[48–51].

A decline in innate and adaptive immunity with aging is referred to as immunosenescence[52]. Immunosenescence induces a pro-inflammatory state and is associated with the susceptibility to autoimmune diseases[53]. In particular, $CD4^+$ T cell immunity is affected by the aging process[54,55]. Although the total number of peripheral T cells is unaffected by aging, $CD4^+$ T cells in the elderly are qualitatively altered; $PD\text{-}1^+$ $CD44^{High}$ $CD4^+$ T cells, which possess the characteristics of cellular senescence such as defective proliferation and a senescence-associated secretory phenotype (SASP), gradually increase with aging[56].

The proteasome plays essential roles in T cell immunity. Proteasome inhibition suppresses the immune-related functions of activated $CD4^+$ T cells, including cell survival, proliferation, and cytokine production[57–59]. However, the regulatory mechanisms underlying the role of the proteasome in $CD4^+$ T cell senescence remain

elusive. In the present study, we showed that proteasome dysfunction triggers a senescence-like phenotype in $CD4^+$ T cells. Induction of the proteasome upon T-cell receptor (TCR) stimulation, rather than the cellular amount of the proteasome at steady state, decreased with age. The results of the study indicate that defective induction of the proteasome is a hallmark of senescence-associated PD-1^+ $CD44^{High}$ $CD4^+$ T cells and underlies T cell senescence.

Results

Impairment of the proteasome induces a senescence-associated phenotype in CD4$^+$ T cells *in vitro*

The effect of proteasome impairment on CD4$^+$ T cell senescence was examined in mouse splenocytes labeled with cell proliferation dye and cultured with immobilized anti-CD3 antibody to stimulate T cell proliferation in the presence or absence of the proteasome inhibitor bortezomib. Reduced proliferation concomitant with the upregulation of cyclin-dependent kinase (CDK) inhibitors is a characteristic of cellular senescence[60]. Flow cytometric analysis showed that bortezomib suppressed the proliferation of CD4$^+$ T cells (Fig. 6a). Consistent with the decreased proliferation, bortezomib treatment upregulated the mRNA expression of the CDK inhibitor *Cdkn1* (encoding p21^{Cip1}) and downregulated the proliferation marker *Mki67* (encoding Ki-67) mRNA (Fig. 6b). Induction of cell cycle-related genes[61] was suppressed in bortezomib-treated cells (Fig. 6c and Supplementary Table 1). These results indicate that the impairment of proteasome activity causes a defect in TCR-mediated proliferation, which is consistent with previous results[57].

The SASP, which is characterized by the secretion of pro-inflammatory factors, is another hallmark of cellular senescence. Secreted phosphoprotein 1 (SPP1, also known as osteopontin) is expressed at higher levels in senescent than in non-senescent CD4$^+$ T cells[56]. RNA-Seq analysis of CD4$^+$ T cells stimulated with anti-CD3 antibody and bortezomib showed increased expression of a series of pro-inflammatory factor genes such as *Spp1*, *Ccl1*, *Ccl3*, *Ccl4*, and *Ccl5* on day 2, and *Gzma*, *Gzmb*, and *Gzmc* on day 5

(Fig. 6d). These results indicate that impairment of proteasome activity induces the SASP in $CD4^+$ T cells.

Increase of senescence-associated PD-1^+ $CD4^+$ T cells in Rpn13-deficient mice

PD-1 expression is one of the major features of T cell senescence *in vivo*[56]. PD-1^+ $CD44^{High}$ $CD4^+$ T cells show senescence-associated phenotypes such as a defect in TCR-mediated proliferation and high production of SPP1[56]. Therefore, we examined whether defects in the proteasome promote $CD4^+$ T cell senescence *in vivo*.

Rpn13 is a ubiquitin receptor and a subunit of the proteasome, and its deletion decreases the degradative capacity of the proteasome[62]. As systemic deletion of Rpn13 causes neonatal lethality[62], we crossed Rpn13-floxed mice with transgenic mice expressing Cre recombinase under control of the Lck promoter to generate T cell-specific Rpn13-deficient mice (Rpn13 Lck-KO). Lck-driven Cre expression alters T cell development in a copy number-dependent manner[63,64]; therefore, we analyzed mice hemizygous for the *Cre* gene. The number of CD4 single positive thymocytes in the thymus was comparable between control and Rpn13 Lck-KO mice, suggesting that $CD4^+$ T cell development is not affected by loss of Rpn13 in T cells (Fig. 7a). A decreased naive T cell pool and increased expression of PD-1 are characteristics of T cell senescence[56]. Although total $CD4^+$ T cell and $CD44^{High}$ $CD62L^{Low}$ memory phenotype $CD4^+$ T cell numbers were comparable between control and Rpn13 Lck-KO mice, the number of $CD44^{Low}$ $CD62L^{High}$ naive $CD4^+$ T cells was significantly reduced in Rpn13 Lck-KO mice (Fig. 7b). The frequency of PD-1^+ $CD44^{High}$ $CD4^+$ T cells was markedly increased

in Rpn13 Lck-KO mice (Fig. 7c). These results indicate that a decrease in proteasome function in T cells induces a typical senescence phenotype in $CD4^+$ T cells *in vivo*.

Strong induction of the proteasome in $CD4^+$ T cells upon TCR stimulation

Gene expression analysis further suggested the involvement of the proteasome in $CD4^+$ T cell senescence. Differentially expressed genes were extracted from RNA-Seq data of $CD4^+$ T cells stimulated with or without anti-CD3 antibody, and Kyoto Encyclopedia of Genes and Genomes pathway enrichment analysis was performed[65]. In addition to genes related to cell cycle regulation and immune responses, proteasome-related genes were highly enriched (Fig. 8a). The 26S proteasome is composed of the catalytic 20S core particle (CP) and the 19S regulatory particle (RP). The CP consists of 14 subunits (α1–7 and β1–7), and the RP comprises 19 subunits (Rpt1–6, Rpn1–3, Rpn5–13, and Rpn15). The assembly of subunits is supported by proteasome assembly chaperones PAC1–4, POMP, S5b, p27, and p28/gankyrin[1,2,66–70]. All the genes encoding CP and RP subunits and most of the genes encoding proteasome assembly chaperones showed approximately two- to four-fold upregulation in stimulated $CD4^+$ T cells compared with non-stimulated $CD4^+$ T cells (Fig. 8b).

To determine whether transcriptional upregulation of proteasome subunit genes led to an increase in functional proteasomes, we measured the activity and protein levels of the proteasome. Cell extracts of an equal number of $CD4^+$ T cells with or without TCR stimulation were subjected to glycerol gradient centrifugation, followed by immunoblot analysis and measurement of peptidase activity in each fraction. The chymotrypsin-like

activity of the 20S and 26S proteasome fractions was considerably higher in stimulated $CD4^+$ T cells than in non-stimulated $CD4^+$ T cells (Fig. 8c, left). Furthermore, as T cells express both constitutive and immunoproteasomes[71], we examined the caspase-like activity, which reflects the activity of constitutive proteasome. This activity was also induced in TCR-stimulated $CD4^+$ T cells (Fig. 8c, right). Consistent with this result, the amount of proteasomes increased in stimulated $CD4^+$ T cells (Fig. 8d). These results indicate that the production of functional proteasomes is strongly induced in TCR-stimulated $CD4^+$ T cells.

Proteasome induction by TCR signaling is mediated by the MEK, IKK, and calcineurin pathways

To investigate the mechanism underlying TCR-mediated proteasome induction, we analyzed public ChIP-Seq data using ChIP-Atlas[72]. The "*in silico* ChIP" in ChIP-Atlas is a tool for identifying binding proteins enriched at a genomic region of interest. Comparison of genomic regions near the translation start sites of proteasome subunits with those of non-proteasomal genes led to the identification of the key component of the AP-1 transcription factor JunD (encoded by *JUND*) as a strong candidate binding protein at proteasome subunit gene loci (Fig. 9a). We assumed that JunD was involved in TCR-mediated induction of the proteasome because JunD is a downstream transcription factor of TCR signaling[73]. Analysis of public ChIP-Seq data[74] confirmed that JunD occupied the promoter region of all proteasome subunits in $CD4^+$ T cells exposed to TCR stimulation in the presence of cytokines *in vitro* (Fig. 9b).

AP-1 is activated through the MEK–ERK–AP-1 pathway[75]. We therefore examined whether this pathway contributes to TCR-mediated upregulation of the proteasome. To this end, we used Rpn11-GFP knock-in reporter mice in which a GFP tag was fused to the 3′ end of the proteasome subunit Rpn11 coding sequence[76]. T cells are a heterogeneous cell population including cells at different stages of activation or differentiation, and this reporter strain enables quantification of proteasomes at the single cell level by measuring GFP fluorescence using flow cytometry. Stimulation of $CD4^+$ T cells from Rpn11-GFP mice with anti-CD3 antibody led to the emergence of a cell population with increased GFP fluorescence (Fig. 9c). To test the involvement of the MEK–ERK–AP-1 pathway, splenocytes from Rpn11-GFP mice were stimulated with anti-CD3 antibody in the presence or absence of the MEK inhibitor AZD6244. TCR-mediated upregulation of the proteasome was suppressed by AZD6244 in a dose-dependent manner, whereas no apparent effect was observed in non-stimulated cells (Fig. 9d). These data suggest that MEK activation contributes to the induction of proteasome transcription upon TCR stimulation.

AZD6244 only partially suppressed TCR-mediated proteasome induction, suggesting that other TCR downstream pathways are involved in proteasome induction. The IKK–NF-κB and calcineurin–NFAT pathways are activated upon TCR stimulation. We therefore inhibited these pathways by treating splenocytes with the IKK inhibitor TPCA-1 and the calcineurin inhibitor cyclosporin A. These chemical inhibitors also partially suppressed TCR-mediated proteasome induction in a dose-dependent manner (Fig. 9e and f). These results suggest that proteasome expression is mediated at least by

MEK, IKK, and calcineurin-dependent pathways, which are upstream of the transcription factors AP-1, NF-κB, and NFAT, respectively.

Defective induction of the proteasome upon TCR stimulation in aged CD4$^+$ T cells

Because proteasome dysfunction caused CD4$^+$ T cell senescence, we hypothesized that the amount of proteasomes decreases with age in CD4$^+$ T cells. However, the levels of Rpn11-GFP in CD4$^+$ T cells did not decrease with age (Fig. 10a). We therefore compared the induction of proteasomes upon TCR stimulation between young (7 weeks) and aged (65 weeks) mice. Rpn11-GFP was highly increased in almost all CD4$^+$ T cells from young mice; however, cells with low proteasome induction (Rpn11-GFP^{low}) accounted for more than half of CD4$^+$ T cells in aged mice (Fig. 10b). The proportion of Rpn11-GFP^{low} CD4$^+$ T cells increased with age (Fig. 10c).

The division of the cell population into Rpn11-GFP^{low} and Rpn11-GFP^{high} groups suggested that the age-related defect in proteasome induction occurred in a specific subpopulation of CD4$^+$ T cells that increases with age. The proportion of PD-1$^+$ CD44^{High} CD4$^+$ T cells increases in an age-dependent manner[56]. This phenomenon was confirmed using Rpn11-GFP mice (Fig. 10d). Cells were sorted into senescence-associated PD-1$^+$ CD44^{High}, memory phenotype PD-1$^-$ CD44^{High}, and naive CD44^{Low} CD62L^{High} CD4$^+$ T cell populations, and cells were stimulated with anti-CD3 antibody. Rpn11-GFP induction was comparable between PD-1$^-$ CD44^{High} and CD44^{Low} CD62L^{High} CD4$^+$ T cells; however, Rpn11-GFP upregulation was not induced in PD-1$^+$ CD44^{High} CD4$^+$ T cells (Fig. 10e). These results indicate that the age-related defect in proteasome

induction is a hallmark of senescence-associated PD-1^{+} CD44^{High} CD4^{+} T cells, and suggest that it underlies T cell senescence.

Discussion

In this study, impairment of the proteasome caused senescence-like phenotypes in $CD4^+$ T cells (Figs. 6 and 7). This was consistent with previous studies showing that proteasome dysfunction leads to premature senescence in different types of cells[45–47]. Proteasome activity declines during aging in several cell types[59]. In $CD4^+$ T cells, however, the expression levels of the proteasome did not decrease with age (Fig. 10a). We speculated that a specific mechanism regulating proteasome expression, rather than a mechanism for maintaining the steady state level of proteasomes, might be involved in $CD4^+$ T cell senescence. We showed that TCR-mediated induction of the proteasome was remarkably impaired in aging cells, and that this impairment was characteristic of PD-1^+ $CD44^{High}$ $CD4^+$ T cells (Fig. 10). TCR-stimulated $CD4^+$ T cells showed defective proliferation and expressed pro-inflammatory genes when exposed to a proteasome inhibitor (Fig. 6), which are characteristics of PD-1^+ $CD44^{High}$ $CD4^+$ T cells[56]. These observations raise the possibility that defects in TCR-mediated induction of the proteasome underlie T cell senescence.

The expression of the proteasome is dynamically induced in response to specific cellular environments[77]. For example, proteasome impairment, feeding, and growth factors induce proteasome expression in a Nrf1-dependent manner[12,41]. Endoplasmic reticulum stress and oxidative stress induce the proteasome via Nrf2[78,79]. Proteasome induction in response to EGF stimulation is mediated by STAT3[80]. The transcription factor FOXO4 increases proteasome activity in embryonic stem cells[40]. However, the mechanism underlying proteasome induction during T cell activation

remains unknown. Here, we showed that proteasome induction was primed by TCR stimulation (Fig. 8). Furthermore, we demonstrated that TCR-mediated proteasome expression was induced via MEK-, IKK-, and calcineurin-dependent pathways (Fig. 9), the involvement of which in regulating proteasome expression has not been considered to date.

Whether all or part of the 33 proteasome subunits are induced is cell type-dependent. All proteasome subunit genes are induced by activated Nrf1 after proteasome impairment[12], whereas induction of a single subunit gene is sufficient for increasing proteasome activity in bone marrow stromal cells and embryonic stem cells[40,81,82]. In the present study, functional proteasomes were remarkably induced by TCR stimulation, concomitant with the transcriptional upregulation of all proteasome subunits (Fig. 8). Binding of the AP-1 component JunD at the promoter region of proteasome subunit genes further suggests that AP-1 mediates the concerted induction of all proteasome subunits (Fig. 9b).

We demonstrated that a defect in TCR-induced proteasome expression is a hallmark of senescence-associated PD-1^{+} CD44^{High} CD4^{+} T cells. However, the mechanism that suppresses TCR-mediated proteasome induction in PD-1^{+} CD44^{High} CD4^{+} T cells remains unknown. PD-1^{+} CD44^{High} CD4^{+} T cells do not show a complete loss of responsiveness to TCR stimulation. PD-1^{+} CD44^{High} CD4^{+} T cells produce pro-inflammatory cytokines and chemokines such as SPP1, CCL3, and CCL4 upon TCR stimulation, whereas they are defective in the production of IL-2 and IL-4[83]. CCAAT enhancer binding protein alpha (C/EBPα) is expressed at high levels in PD-1^{+} CD44^{High}

$CD4^+$ T cells, and overexpression of C/EBPα suppresses IL-2 production and induces SPP1 in response to TCR[56]. In addition, most of the proteasome genes have the CCAAT box in their promoters[84]. Therefore, C/EBPα might suppress the TCR-mediated induction of the proteasome in PD-1^+ $CD44^{High}$ $CD4^+$ T cells. Another possibility is partial attenuation of TCR signaling pathways, including MEK–ERK-, IKK–NF-κB-, and calcineurin–NFAT-dependent pathways. Stimulated PD-$1^+$$CD44^{High}$ $CD4^+$ T cells exhibit normal ERK activation, which is downstream of MEK[56]. On the other hand, an age-related decline in calcineurin activity in rat T cells and NF-κB induction in human T cells was reported[85,86]. Accordingly, age-related defect of proteasome induction might attribute to impairment of IKK–NF-κB-, and calcineurin–NFAT-dependent pathways.

Senescent cells may lead to a pro-inflammatory state through the acquisition of SASP[53]. Senescence-associated $CD4^+$ T cells accumulate in the visceral adipose tissue of obese mice fed a high-fat diet, and lead to insulin resistance by producing pro-inflammatory factors[87]. Whether the failure of proteasome induction is a cause or a result of T cell senescence is currently unknown. Elucidation of the mechanisms underlying TCR-mediated proteasome induction and the failure of proteasome induction in senescent T cells may provide a target for the treatment of age-related diseases associated with inflammation.

Figures and figure legends

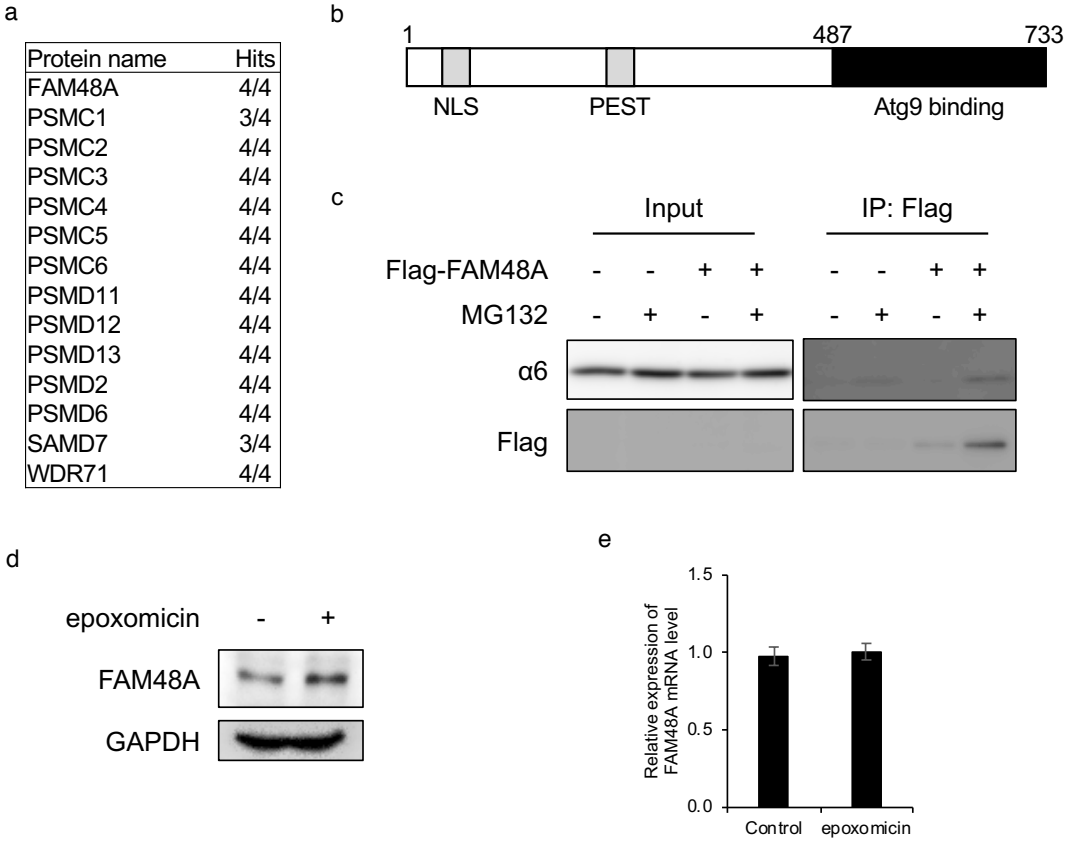

FIGURE 1 FAM48A is identified as a proteasomal substrate and proteasome associated protein.
(a) List of proteins that were identified by LC-MS/MS analysis of co-immunoprecipitation of Flag-tagged p28 from 1% NP40-soluble fraction of HEK293T cells. The numbers of hits among the four experiments are shown. (b) Domain organization of full-length FAM48A. FAM48A is predicted to have a nuclear localization signal (NLS), a PEST domain, and a region for interaction with Atg9. (c) Flag-tagged FAM48A was transfected into HEK293T cells treated with 10 μM MG132. Cell extracts were immunoprecipitated with M2 agarose and analyzed by immunoblotting. (d) U2OS cells were treated with 1 μM epoxomicin for 3 h. Cell extracts were immunoblotted with anti-FAM48A and anti-GAPDH antibodies. (e) FAM48A mRNA levels in cells in (d) were quantified by RT-qPCR in triplicate. mRNA levels of FAM48A were normalized by GUSB mRNA levels. Data are presented as mean ± s.d.

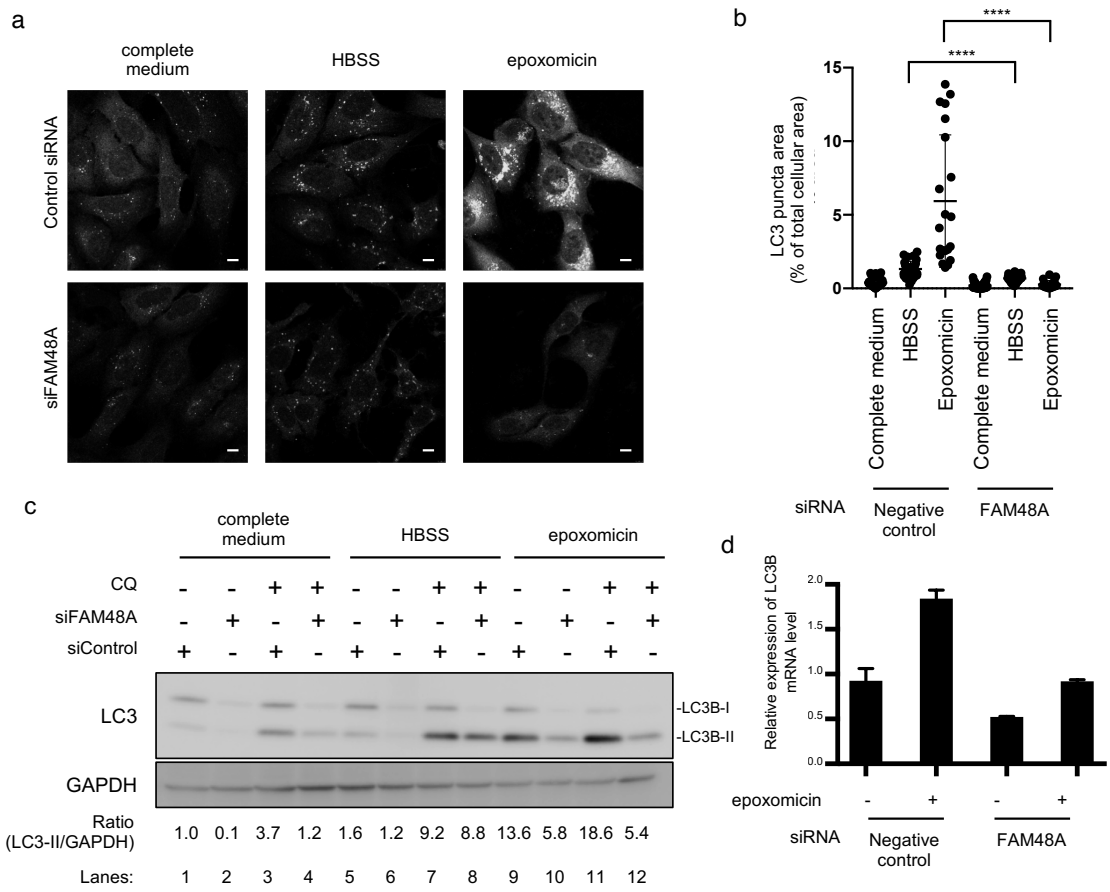

FIGURE 2 FAM48A regulates compensatory autophagy upon proteasome dysfunction. (a) U2OS cells were transfected with control siRNA or FAM48A siRNA and cultured in complete medium, HBSS, for 1.5 h, or complete medium containing 25 nM epoxomicin for 18 h. Cells were immunostained using anti-LC3 antibodies. Scale bars: 10 μm. (b) The ratio of the total area of LC3-positive puncta to the total cellular area was quantified using ImageJ. Data are presented as mean ± s.d. Statistical analyses for negative control HBSS (n = 33 cells) versus FAM48A siRNA HBSS (n = 19 cells) (****P< 0.001), and negative control epoxomicin (n = 21 cells) versus FAM48A siRNA epoxomicin (n = 19 cells) (****P < 0.001) were conducted with unpaired t-test with Welch's correction. (c) U2OS cells were transfected with control or FAM48A siRNA and cultured in complete medium, HBSS, for 1.5 h, or complete medium containing 50 nM epoxomicin for 18 h with 20 μM CQ for 1.5 h. Cell extracts were subjected to immunoblot analysis using anti-LC3 and GAPDH antibodies. (d) LC3B mRNA levels in U2OS cells were quantified by RT-qPCR in triplicate. mRNA levels of FAM48A were normalized by GUSB mRNA levels. Cells were cultured in complete medium or complete medium containing 50 nM epoxomicin for 18 h. Data are presented as mean ± s.d.

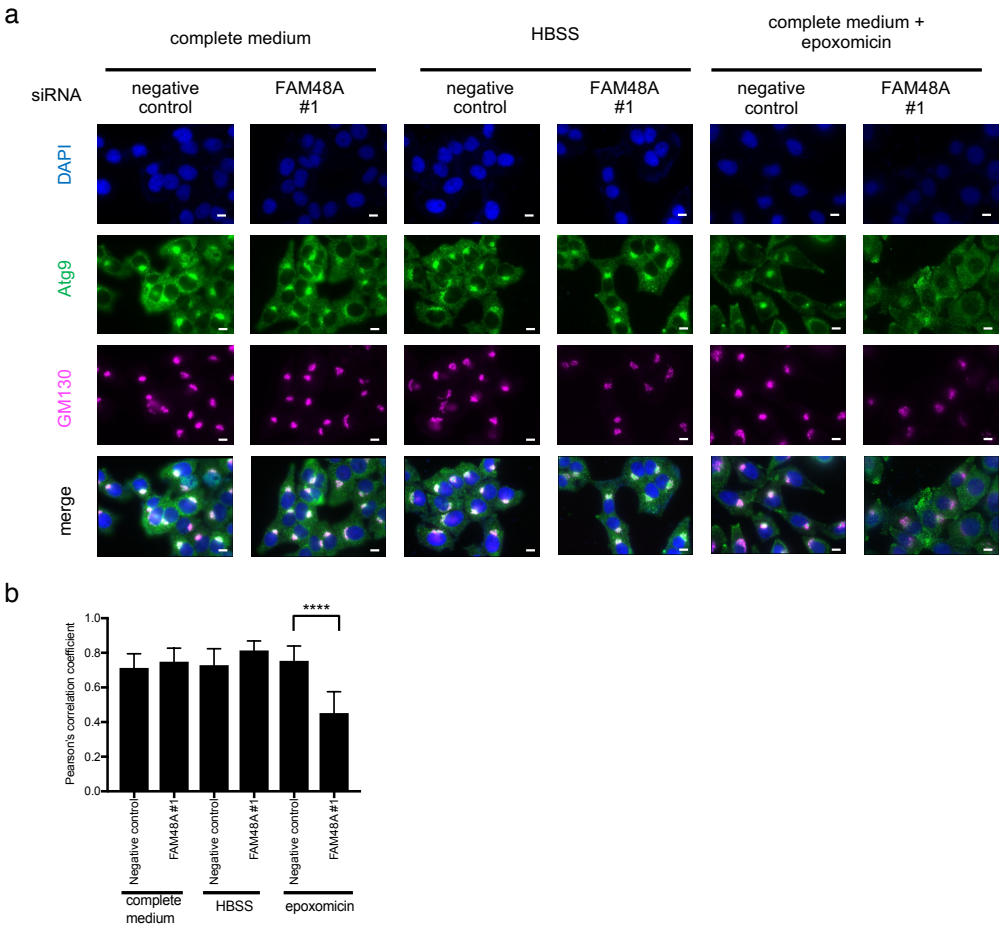

FIGURE 3 FAM48A is required for localization of Atg9 in TGN upon proteasome inhibition. (a) U2OS cells were transfected with control siRNA or FAM48A siRNA. Cells were incubated in complete medium, HBSS, for 1.5 h, or complete medium containing 50 nM epoxomicin for 18 h and stained with anti-Atg9 and anti-GM130 antibodies. Scale bars: 10 μm. (b) Co-localization of Atg9 and GM130 in (a) was quantified using ImageJ. Data are presented as mean ± s.d. Statistical analysis for negative control epoxomicin (n = 17 cells) versus FAM48A siRNA epoxomicin (n = 16 cells) (****$P < 0.001$) was conducted with unpaired t-test with Welch's correction.

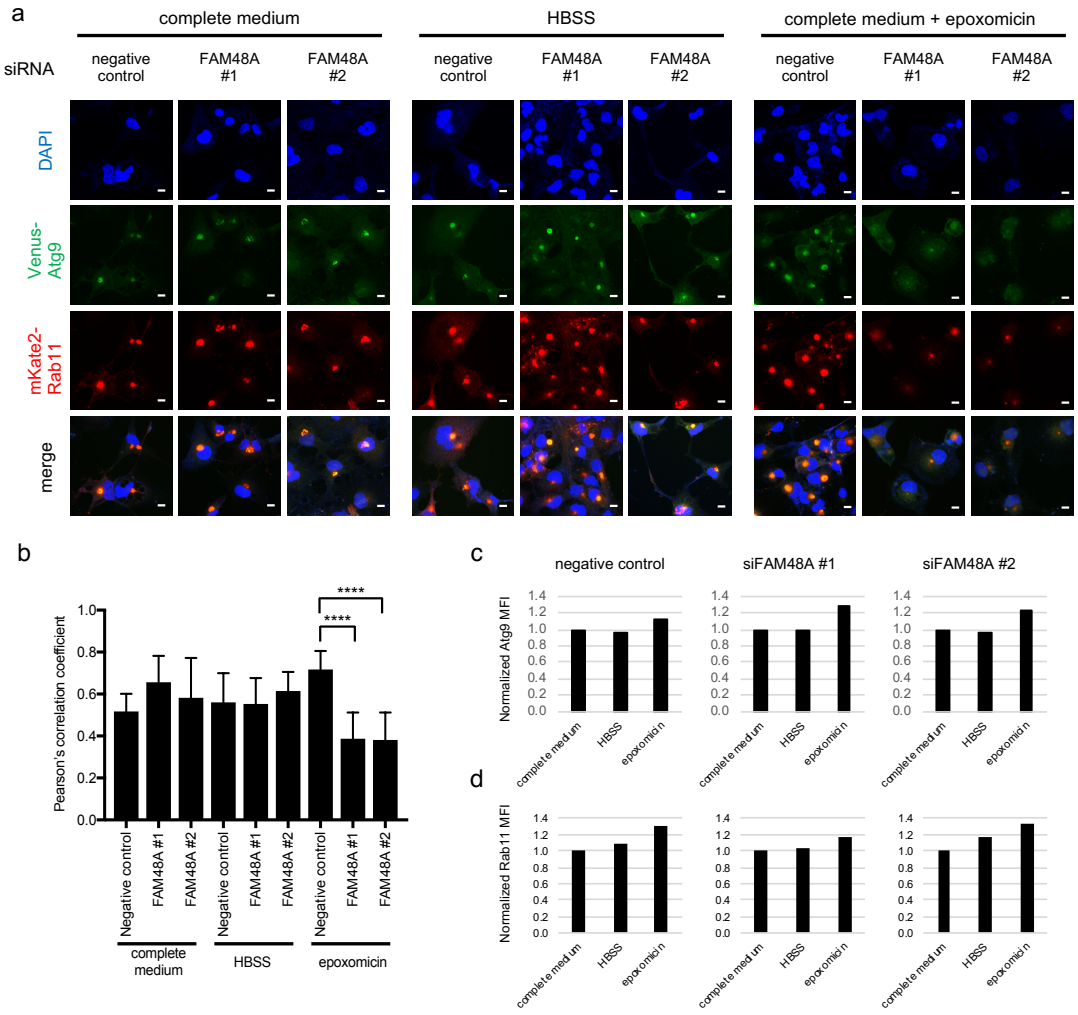

FIGURE 4 FAM48A is required for localization of Atg9 on recycling endosomes upon proteasome inhibition. (a) COS-1 cells stably expressing Venus-Atg9 and mKate2-Rab11 were transfected with control siRNA or either of two FAM48A siRNAs. Cells were cultured in complete medium, HBSS, for 1.5 h, or complete medium containing 50 nM epoxomicin for 18 h and then visualized by fluorescence microscopy. Scale bars: 10 μm. (b) Co-localization of Venus-Atg9 and mKate2-Rab11 in (a) was quantified using ImageJ. Data are presented as mean ± s.d. Statistical analyses for negative control epoxomicin (n = 32 cells) versus FAM48A #1 siRNA epoxomicin (n = 16 cells) or FAM48A #2 siRNA epoxomicin (****P < 0.001) were conducted with unpaired t-test with Welch's correction. (c, d) Flow cytometric analysis of cells in (a). Median fluorescence intensity (MFI) of Venus-Atg9 (d) and mKate2-Rab11 (d) were normalized to those in control medium.

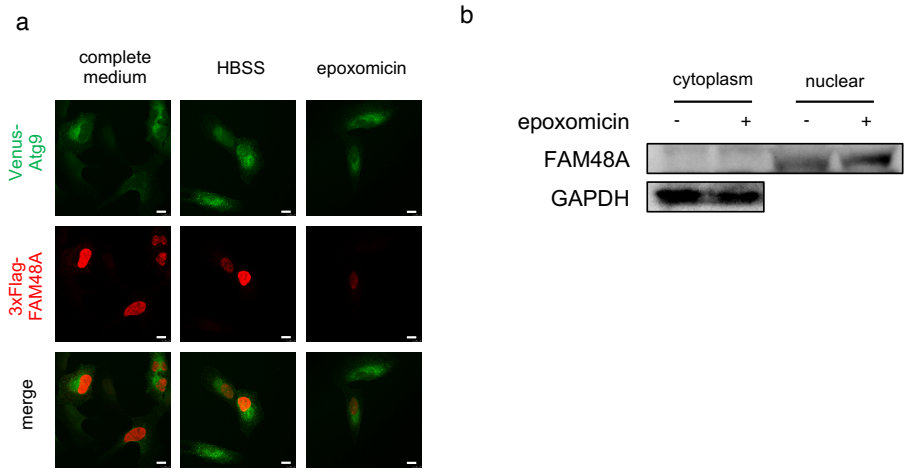

FIGURE 5 FAM48A accumulated in the nucleus during proteasome inhibition. (a) U2OS cells stably expressing Venus-Atg9 were transfected with 3×Flag-FAM48A. Cells were cultured in complete medium, HBSS, for 1.5 h, or complete medium containing 50 nM epoxomicin for 18 h. Flag-FAM48A was probed with an anti-Flag antibody. Scale bars: 10 μm. (b) U2OS cells were treated with 10 μM epoxomicin for 3 h. Cell homogenates were fractionated into the cytoplasm and nucleus by centrifugation. Fractionated samples were subjected to immunoblot analysis with anti-FAM48A and anti-GAPDH antibodies.

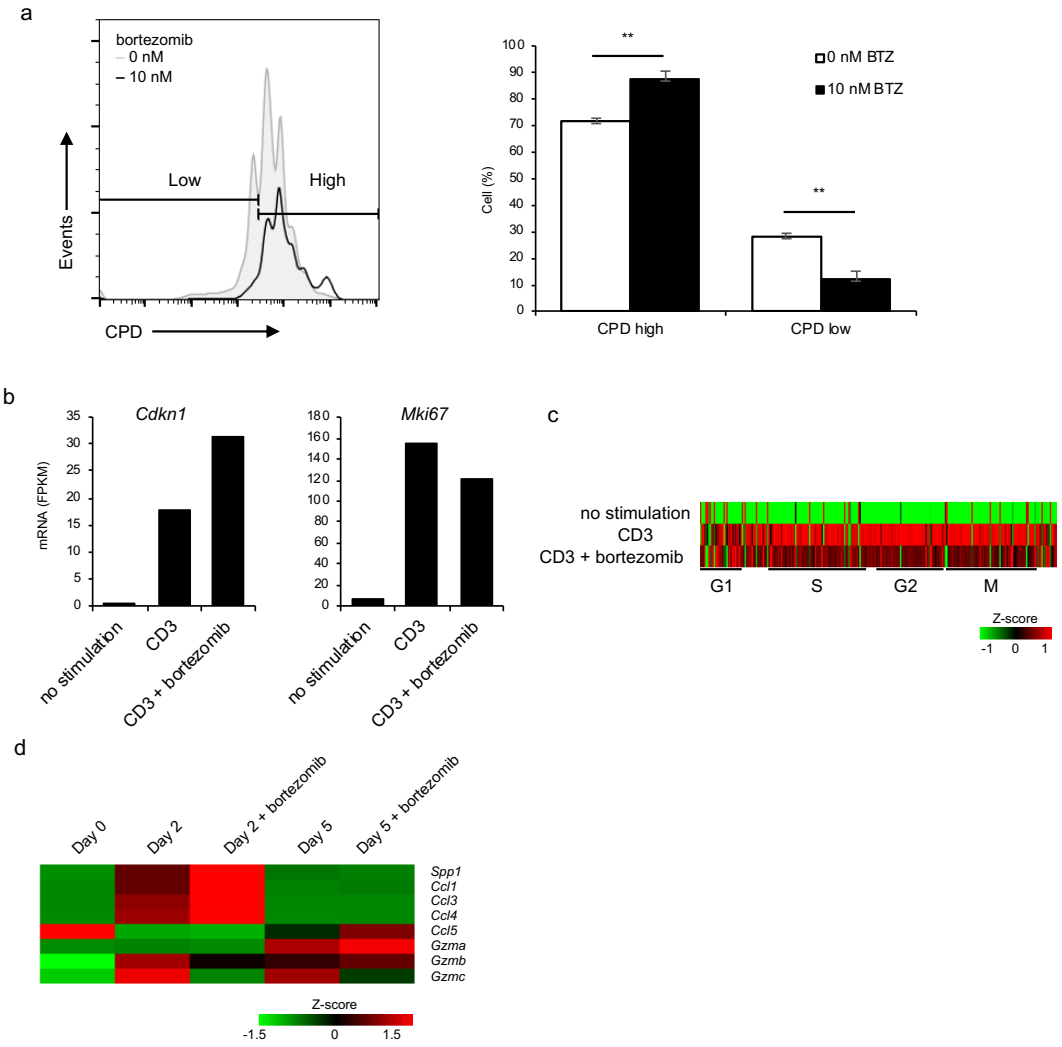

Figure 6 CD4⁺ T cells treated with bortezomib exhibit characteristics of cellular senescence. (a) Flow cytometric analysis of CD4⁺ T cells stained with cell proliferation dye (CPD) and cultured with plate-bound anti-CD3 antibody and the indicated concentration of bortezomib. Histograms (left) and frequency of CPD high and low staining (right) in CD4⁺ T cells are shown (n = 3; mean ± SD). (b, c) RNA-Seq analysis of purified CD4⁺ T cells stimulated with plate-bound anti-CD3 antibody in the presence or absence of bortezomib for 5 days. Panel b shows the fragments per kilobase per million mapped reads (FPKM) value for *Cdkn1a* and *Mki67*. Panel c shows a heatmap of the Z-score of cell cycle-related genes. (d) RNA-Seq analysis of purified CD4⁺ T cells stimulated with plate-bound anti-CD3 antibody in the presence or absence of bortezomib for 2 or 5 days. A heatmap of the Z-score of SASP-related genes is shown. **P < 0.01 (Student's t-test).

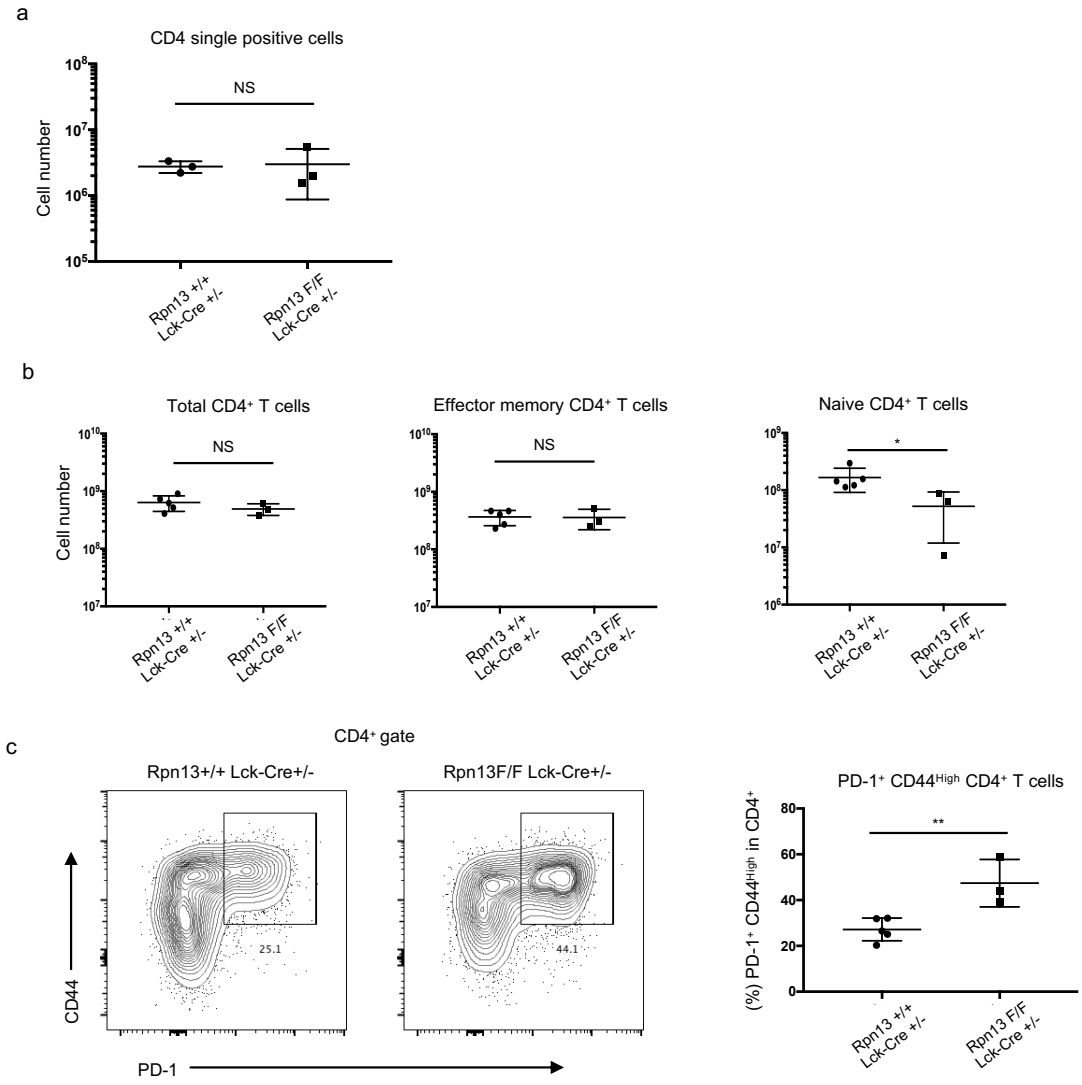

Figure 7 Increase in PD-1^{+} CD44^{High} CD4^{+} T cells in Rpn13-deficient mice.
(a) Number of CD4 single positive cells in the thymus (n = 3; mean ± SD) of control and Rpn13 Lck-KO mice. (b) Number of total CD4^{+} T cells, CD44^{Low} CD62L^{High} naive CD4^{+} T cells, and CD44^{High} CD62L^{Low} effector memory CD4^{+} T cells in the spleen of control and Rpn13 Lck-KO mice (n = 3–5; mean ± SD). (c) Representative flow cytometric profiles of CD4^{+} T cells (left) and frequency of PD-1^{+} CD44^{High} cells among CD4^{+} T cells of control and Rpn13 Lck-KO mice (n = 3–5; mean ± SD). *P < 0.05, **P < 0.01 (Student's t-test).

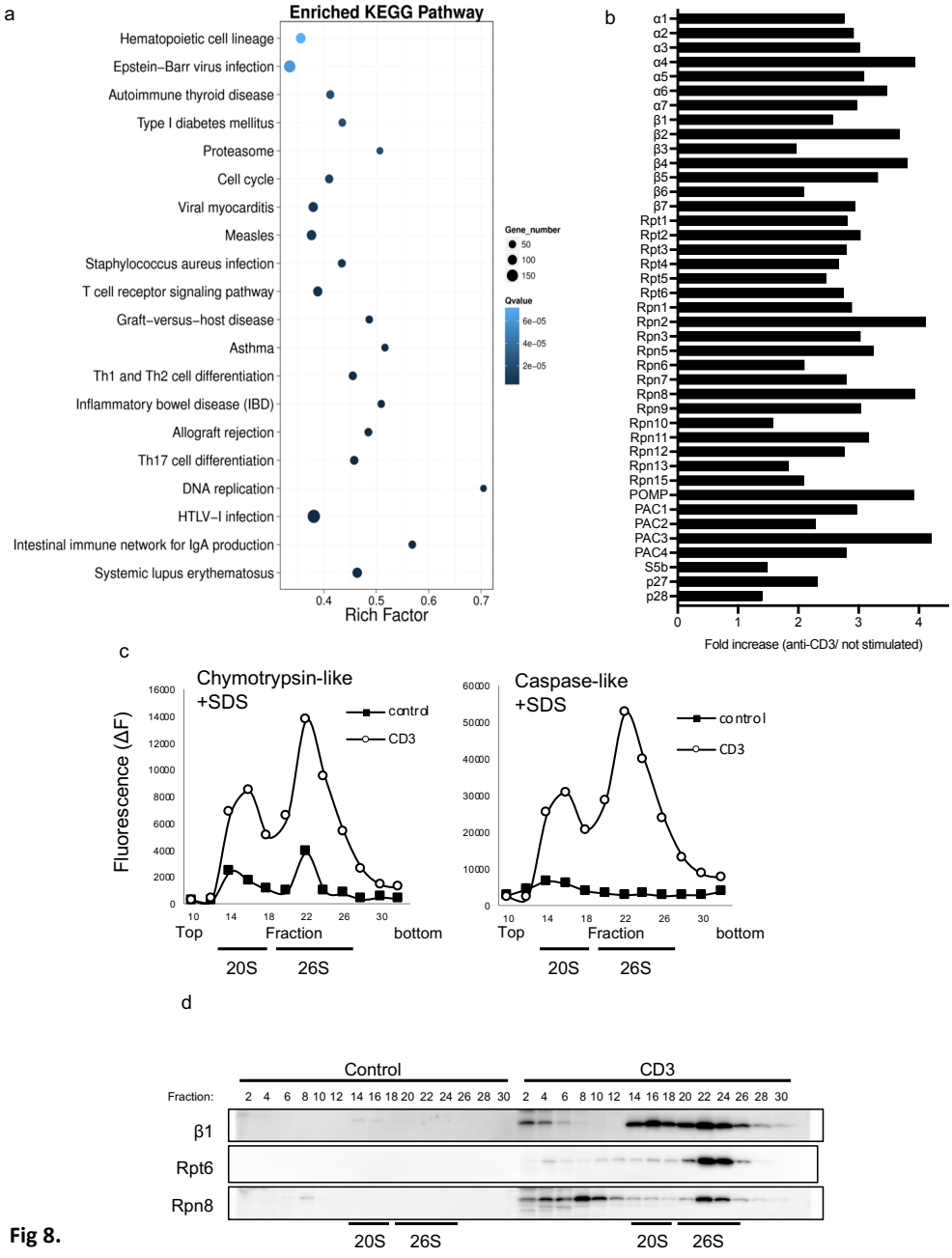

Fig 8.

Figure 8 Induction of the proteasome in CD4⁺ T cells upon TCR stimulation.
(a, b) RNA-Seq analysis of CD4⁺ T cells cultured with and without anti-CD3 antibody for 2 days. Panel a shows the enriched KEGG pathway analysis of differentially expressed genes (DEGs). The color indicates the q-value (high: white, low: blue). The point size indicates DEG number. Panel b shows the relative mRNA expression of genes encoding proteasome subunits and assembly chaperones in CD4⁺ T cells cultured with and without anti-CD3 antibody. (c) Extracts of CD4⁺ T cells cultured with or without anti-CD3 antibody were fractionated by 8–32% glycerol gradient centrifugation into 32 fractions from the top. Suc-LLVY-MCA (left) and Z-LLE-MCA (right) hydrolytic activities were measured in the presence of 0.02% SDS. 20S: 20S proteasome; 26S: 26S proteasome. (d) Immunoblotting of the fractionated lysates prepared in c. Data are representative of three independent experiments.

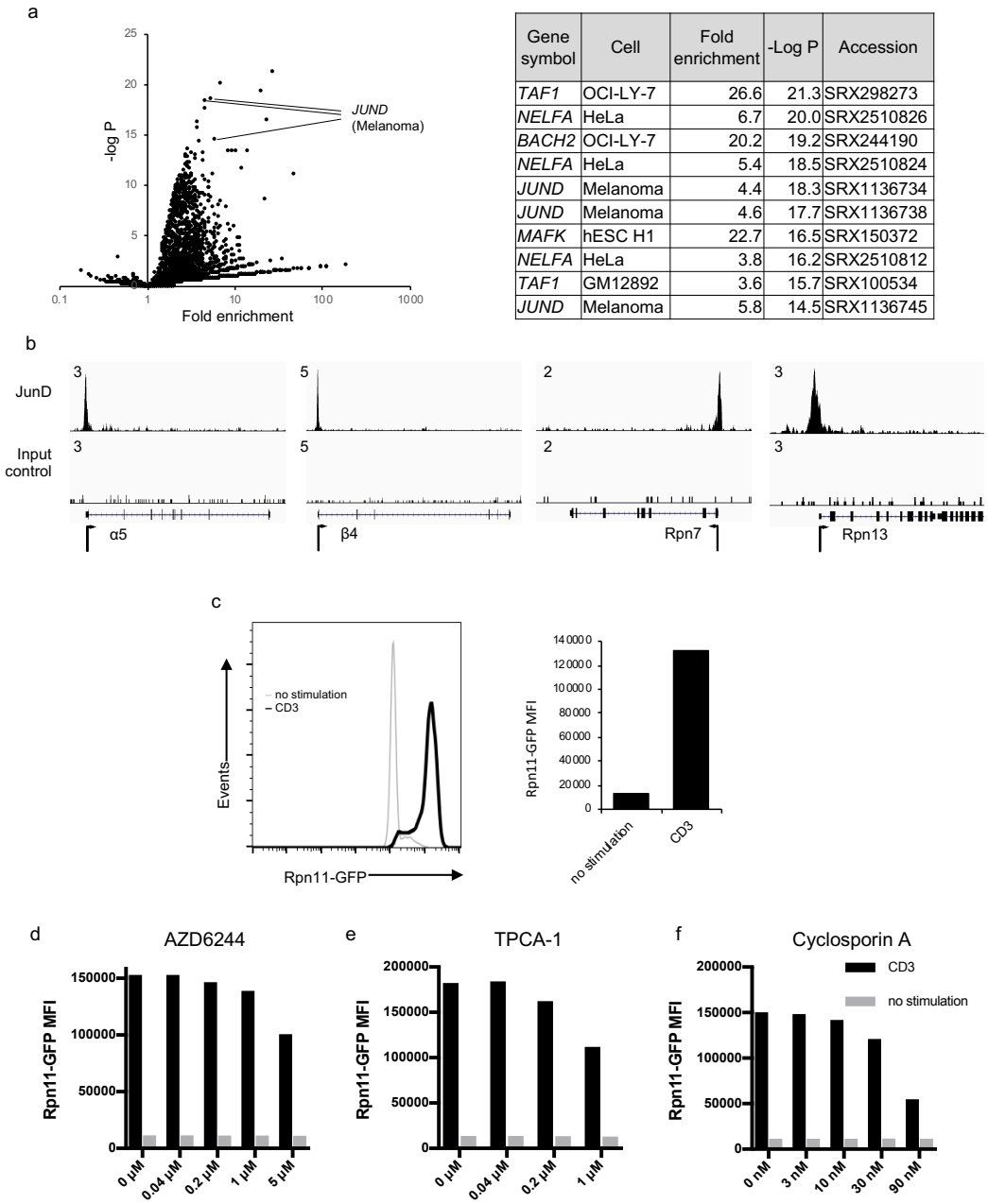

Gene symbol	Cell	Fold enrichment	-Log P	Accession
TAF1	OCI-LY-7	26.6	21.3	SRX298273
NELFA	HeLa	6.7	20.0	SRX2510826
BACH2	OCI-LY-7	20.2	19.2	SRX244190
NELFA	HeLa	5.4	18.5	SRX2510824
JUND	Melanoma	4.4	18.3	SRX1136734
JUND	Melanoma	4.6	17.7	SRX1136738
MAFK	hESC H1	22.7	16.5	SRX150372
NELFA	HeLa	3.8	16.2	SRX2510812
TAF1	GM12892	3.6	15.7	SRX100534
JUND	Melanoma	5.8	14.5	SRX1136745

Figure 9 Induction of the proteasome in CD4$^+$ T cells thorough TCR signaling pathways.
(a) "In silico ChIP" analysis based on constitutive proteasome subunits. A scatter plot (left) and list of the top 10 genes with the lowest -log P value (right) are shown. Fold enrichment represents the ratio of the foreground value [the number of detected peaks near the transcription start site (TSS) of genes encoding constitutive proteasome subunits] to the background value (total number of detected peaks near TSSs of all genes). The p-value represents the significance of the overlap between the foreground value and background value. (b) Alignment of JunD and IgG (input control) reads in CD4$^+$ T cells stimulated with TCR and treated with cytokine at the representative proteasome subunit gene loci. Arrowheads indicate gene orientation. (c–f) Splenocytes from Rpn11-GFP/+ mice were cultured with or without plate-bound anti-CD3 antibody. Panel c shows a representative histogram (left) and the mean fluorescence intensity (MFI) of Rpn11-GFP (right) of CD4+ T cells. Panels d–f show cells cultured with the indicated inhibitors, (d) AZD6244, (e) TPCA-1, and (f) cyclosporin A, at several concentrations for 2 days. The MFI of Rpn11-GFP in CD4$^+$ T cells is shown. Data are representative of three independent experiments.

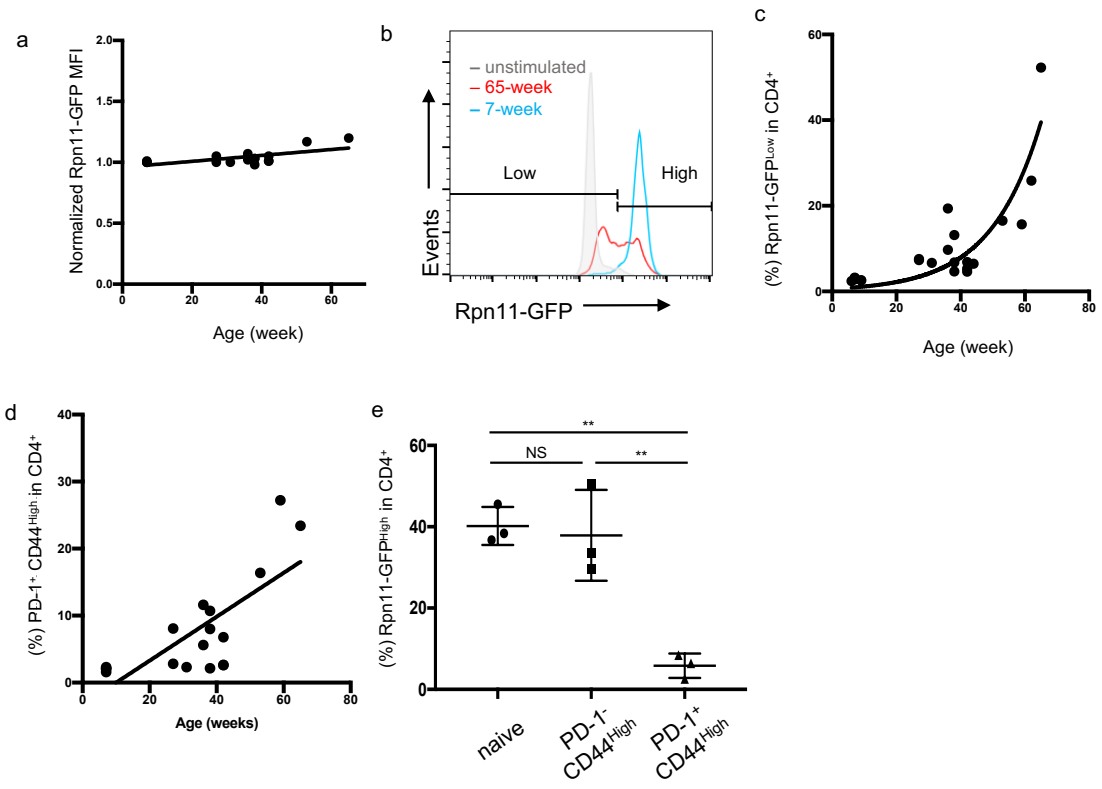

Figure 10 Defect in TCR-mediated induction of the proteasome in CD4$^+$ T cells in the PD-1$^+$ CD44^{High} CD4$^+$ T cell population

(a) The Rpn11-GFP MFI value in CD4$^+$ T cells from Rpn11-GFP/+ mice of various ages was normalized to that at 6-weeks old. (b, c) Splenocytes from Rpn11-GFP/+ mice of various ages were cultured with plate-bound anti-CD3 antibody. (b) Representative histogram and (c) frequency of Rpn11-GFP^{Low} CD4$^+$ T cells are shown. (d) Frequency of PD-1$^+$ CD44^{High} CD4$^+$ T cells among CD4$^+$ T cells from Rpn11-GFP/+ mice of various ages. (e) Sorted CD44^{Low} CD62L^{High} naive CD4$^+$ T cells, PD-1$^-$ CD44^{High} CD4$^+$ T cells, and PD-1$^+$ CD44^{High} CD4$^+$ T cells were cultured with plate-bound anti-CD3 antibody for 2 days. Frequency of Rpn11-GFP^{High} cells among CD4$^+$ T cells are shown (n = 3). **P < 0.01 (one-way ANOVA followed by Tukey's test).

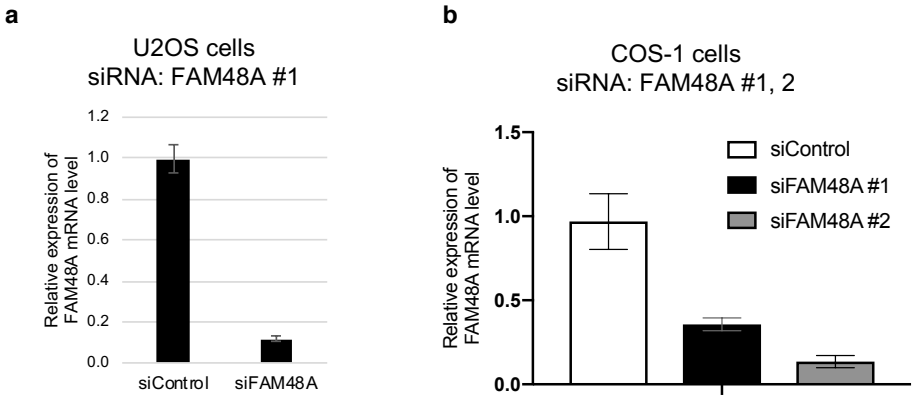

Supporting Information Figure S1 Knockdown efficiency of FAM48A by siFAM48A. (a, b) FAM48A mRNA levels in U2OS cells (a) and COS-1 cells (b) were quantified by RT-qPCR in triplicate. mRNA levels of FAM48A were normalized by GUSB mRNA levels. Data are presented as mean ± s.d.

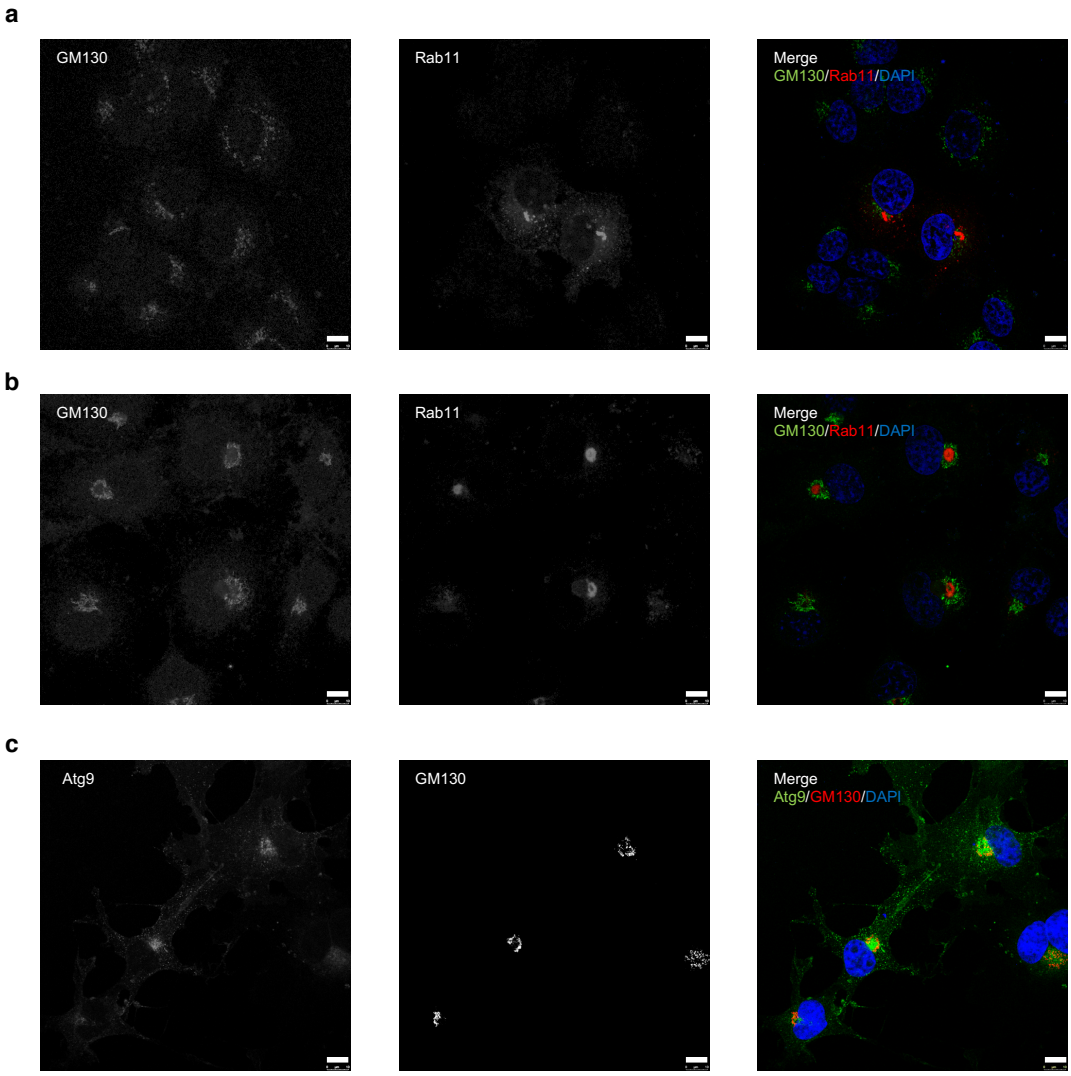

Supporting Information Figure S2 Localization of GM130, Rab11, and Atg9 in U2OS and COS-1 cells. (a) U2OS cells transiently expressing mKate2-Rab11. (b) COS-1 cells stably expressing mKate2-Rab11. (c) COS-1 cells stably expressing Venus-Atg9 and mKate2-Rab11. Cells were cultured in complete medium and stained with anti-GM130 antibodies and DAPI (a-c). Scale bars: 10 μm.

GENE SYMBOL	no stimulation	CD3	CD3 +bortezomib
ARGLU1	0.90	-1.39	0.50
Armt1	-1.39	0.92	0.47
CASP8AP2	-1.35	1.05	0.30
CCT4	-1.40	0.55	0.85
CSK	1.37	-0.40	-0.98
CSTF2T	1.21	0.03	-1.24
DHX29	-0.66	-0.76	1.41
GPR107	1.38	-0.97	-0.41
GRPEL1	-1.41	0.75	0.66
GSPT1	-1.40	0.52	0.88
Hilpda	1.38	-0.42	-0.96
HSPA4	-1.36	0.33	1.02
IMPAD1	-1.39	0.49	0.90
KHDRBS1	-1.41	0.63	0.78
MAPK1	-1.41	0.81	0.59
MTCH1	-1.40	0.87	0.53
PANK2	-1.38	0.96	0.42
PLCXD1	1.36	-1.01	-0.36
PLEKHA2	-0.99	1.37	-0.38
PTP4A2	1.24	-0.02	-1.21
RER1	-1.41	0.80	0.61
RNF138	-1.40	0.52	0.88
SLBP	-1.37	0.99	0.38
SNRPA	-1.37	0.37	1.00
SRP19	-1.41	0.67	0.75
SRP72	-1.37	0.38	0.99
SYNCRIP	-1.41	0.77	0.64
SYNCRIP	-1.41	0.77	0.64
TSPYL4	-1.22	-0.01	1.23
U2surp	-1.39	0.92	0.47
ARGLU1	0.90	-1.39	0.50

BARD1	-1.36	1.02	0.33
C1GALT1	1.40	-0.51	-0.89
CDC25A	-1.38	0.97	0.40
DTL	-1.40	0.89	0.51
E2F1	-1.41	0.84	0.57
EIF2S1	-1.41	0.81	0.60
FN3KRP	-1.31	0.18	1.12
GINS2	-1.38	0.97	0.41
Hnrnpd	-1.36	1.03	0.33
IVNS1ABP	1.41	-0.70	-0.71
MBD4	-1.35	1.04	0.32
MCM6	-1.39	0.90	0.49
NASP	-1.38	0.96	0.42
PANK2	-1.38	0.96	0.42
PNN	-1.35	0.30	1.05
SENP5	-1.33	1.07	0.26
SIVA1	-1.39	0.94	0.45
STAM	1.41	-0.68	-0.73
2810417H13Rik	-1.37	1.00	0.37
ABHD5	-1.27	0.10	1.17
APEX2	-1.39	0.47	0.92
ASF1B	-1.39	0.94	0.45
ATAD2	-1.36	1.01	0.36
BLM	-1.39	0.92	0.48
BRCA1	-1.38	0.96	0.42
CASP2	-1.41	0.77	0.64
CCND3	-1.37	0.99	0.38
CCT4	-1.40	0.55	0.85
CDC6	-1.37	0.98	0.40
CDK2	-1.38	0.97	0.41
CENPQ	-1.32	1.11	0.21
Cenpu	-1.38	0.97	0.41

CHAF1B	-1.40	0.87	0.53
DCK	-1.34	1.06	0.28
DHFR	-1.41	0.82	0.59
DONSON	-1.34	1.07	0.27
Dscc1	-1.41	0.83	0.58
DUSP6	0.08	-1.26	1.18
EED	-1.03	1.36	-0.33
EXO1	-1.40	0.87	0.53
EZH2	-1.40	0.86	0.54
FANCA	-1.41	0.76	0.65
FANCG	-1.36	1.02	0.34
FANCI	-1.37	1.00	0.37
FEN1	-1.39	0.92	0.47
GINS3	-1.37	0.99	0.39
GMNN	-1.39	0.92	0.47
GPD2	1.37	-1.00	-0.36
HAT1	-1.38	0.96	0.42
HELLS	-1.37	1.00	0.37
Hspb11	-1.22	1.23	-0.01
ICMT	-1.41	0.60	0.81
KNTC1	-1.39	0.91	0.49
MCM4	-1.39	0.91	0.48
MIS12	-1.37	0.99	0.37
MSH2	-1.41	0.82	0.59
MYCBP	-1.37	0.37	1.00
NRD1	1.04	-1.35	0.31
NUP43	-1.40	0.88	0.52
ORC1	-1.41	0.81	0.59
ORC6	-1.40	0.89	0.51
PCNA	-1.36	1.02	0.33
PKMYT1	-1.36	1.01	0.35
POLD3	-1.37	0.99	0.38

POLE	-1.38	0.94	0.44
PRIM2	-1.37	0.99	0.38
RBBP8	-1.37	1.00	0.37
RFC2	-1.40	0.85	0.55
RFC3	-1.38	0.95	0.43
RFC4	-1.39	0.93	0.45
RMI1	-1.41	0.70	0.71
RPA2	-1.40	0.89	0.50
Rprd2	1.39	-0.90	-0.50
RRM1	-1.37	0.99	0.38
RRM2	-1.39	0.92	0.47
RSRC2	1.40	-0.89	-0.51
RUSC1	-0.57	-0.84	1.41
SAR1B	-1.41	0.81	0.60
SEC23B	-1.40	0.88	0.52
SETD3	-1.40	0.89	0.50
SH3GLB1	-1.39	0.93	0.46
Ska1	-1.41	0.82	0.59
STOML1	0.98	-1.37	0.39
TMEM106C	-0.05	1.25	-1.20
TOPBP1	-1.40	0.89	0.51
Ubr7	-1.39	0.90	0.49
USP1	-1.38	0.97	0.41
YWHAH	-1.34	1.05	0.29
AURKB	-1.38	0.94	0.44
CDC7	-1.40	0.87	0.54
ERCC6L	-1.39	0.93	0.45
HIRIP3	-1.40	0.85	0.55
NUP50	-1.38	0.97	0.41
STIL	-1.39	0.94	0.45
UMPS	-1.41	0.84	0.57
ARHGDIB	-1.34	1.07	0.27

AURKB	-1.38	0.94	0.44
Bora	-1.38	0.96	0.42
CASP3	-1.39	0.47	0.92
CCNA2	-1.38	0.96	0.42
CCNF	-1.38	0.96	0.42
CDC25C	-1.40	0.88	0.52
CDCA3	-1.37	0.98	0.39
CDCA8	-1.39	0.90	0.49
CDKN2C	-1.39	0.91	0.49
CENPA	-1.39	0.91	0.48
CEP76	-1.41	0.78	0.63
CKAP2	-1.38	0.96	0.42
CKS1B	-1.39	0.90	0.49
DTYMK	-1.38	0.95	0.43
Dtymk	-1.38	0.95	0.43
FZR1	-1.39	0.93	0.45
GABPB2	-0.34	1.36	-1.02
H2AFX	-1.35	1.04	0.31
HJURP	-1.39	0.93	0.46
HMGB2	-1.37	1.00	0.37
KIF11	-1.38	0.97	0.40
KIF23	-1.36	1.02	0.34
KIFC1	-1.40	0.89	0.51
KPNA2	-1.39	0.94	0.45
Kpna2	-1.39	0.94	0.45
LMNB1	-1.38	0.97	0.41
MAD2L1	-1.38	0.96	0.42
MELK	-1.36	1.02	0.33
Mis18bp1	-1.37	0.99	0.38
MKI67	-1.38	0.95	0.44
NCAPG2	-1.36	1.01	0.35
NCAPH	-1.39	0.94	0.45

NEIL3	-1.38	0.94	0.44
NUSAP1	-1.34	1.05	0.29
OXSR1	-1.32	0.21	1.11
PPP1R12A	-1.40	0.90	0.50
PPP1R2	-1.04	1.35	-0.31
PSMD11	-0.96	-0.42	1.38
PSRC1	-1.38	0.44	0.95
RANGAP1	-1.38	0.97	0.41
SHCBP1	-1.38	0.96	0.42
SMC4	-1.25	1.20	0.06
TOP2A	-1.37	0.98	0.40
TTK	-1.38	0.96	0.41
TUBA4A	-1.38	0.95	0.44
Tubb4b	-1.39	0.90	0.49
TUBD1	-1.40	0.50	0.89
UBE2C	-1.38	0.95	0.44
Agfg1	0.53	0.87	-1.40
Ago2	1.29	-0.14	-1.15
ANP32E	-1.35	1.04	0.31
ARHGAP19	-1.33	1.08	0.25
ARL6IP1	-1.38	0.95	0.43
AURKA	-1.40	0.85	0.55
BIRC5	-1.38	0.97	0.40
BUB1	-1.37	0.98	0.40
BUB1B	-1.38	0.96	0.41
CBX3	-1.33	1.09	0.23
CCNB2	-1.38	0.95	0.43
CDC27	-1.40	0.85	0.56
CDCA3	-1.37	0.98	0.39
CENPE	-1.39	0.91	0.48
CENPF	-1.36	1.01	0.36
CEP55	-1.37	0.99	0.38

CKAP2	-1.38	0.96	0.42
CKAP5	-1.37	0.98	0.40
CKS2	-1.40	0.89	0.50
DHX57	1.35	-1.03	-0.32
Dlgap5	-1.40	0.90	0.50
ECT2	-1.37	0.98	0.39
FAM216A	-1.35	1.03	0.32
FAM64A	-1.37	1.00	0.37
FZR1	-1.39	0.93	0.45
GTSE1	-1.41	0.64	0.77
HMGB3	-1.37	0.98	0.39
HMMR	-1.40	0.87	0.53
HN1	-1.35	1.04	0.31
KIF14	-1.38	0.96	0.42
Kif20b	-1.40	0.89	0.51
KIF2C	-1.39	0.91	0.48
KIF5B	1.40	-0.51	-0.88
Kpna2	-1.39	0.94	0.45
MCM4	-1.39	0.91	0.48
NEK2	-1.37	0.98	0.39
NUSAP1	-1.34	1.05	0.29
PBK	-1.34	1.07	0.27
PLK1	-1.37	0.98	0.39
PPIF	1.40	-0.54	-0.86
PPP2CA	-1.28	1.16	0.12
PRC1	-1.38	0.95	0.43
PRR11	-1.38	0.97	0.41
QSER1	-1.41	0.61	0.80
RAD51C	-1.31	1.12	0.20
RAN	-1.41	0.83	0.58
RANGAP1	-1.38	0.97	0.41
RCAN1	-1.17	-0.10	1.27

RNF126	-0.71	-0.71	1.41
SFPQ	-1.24	1.21	0.04
SMC4	-1.25	1.20	0.06
SMTN	-1.33	1.07	0.26
SPAG5	-1.38	0.96	0.41
Spdl1	-1.40	0.89	0.50
TPX2	-1.38	0.95	0.43
TRAIP	-1.38	0.97	0.41
TROAP	-1.38	0.97	0.41
TSN	-1.39	0.93	0.45
WAPAL	0.69	0.72	-1.41
WDR77	1.19	-1.25	0.06
YWHAH	-1.34	1.05	0.29
A430005L14Rik	-1.31	1.11	0.20
CDKN3	-1.38	0.95	0.43
CENPI	-1.37	0.99	0.38
DHX16	-0.76	-0.65	1.41
DKC1	-1.41	0.79	0.62
DYNLL1	-0.92	1.39	-0.47
FUBP1	-1.41	0.74	0.67
GSPT1	-1.40	0.52	0.88
HERC4	1.40	-0.50	-0.90
HSPA8	-1.41	0.71	0.71
LSM5	-0.94	1.38	-0.44
Nop16	-1.36	0.36	1.01
NUP98	-1.41	0.61	0.80
PPP2R2A	-1.04	-0.32	1.35
PTTG1	1.40	-0.89	-0.51
RBM8A	-1.26	1.18	0.08
SEPHS1	-1.35	1.04	0.31
SYNCRIP	-1.41	0.77	0.64
TAF9	-1.41	0.70	0.72

Supporting Table 1

Z-score of gene expression of cell cycle-related genes.

Materials and methods (Part A)

DNA constructs

cDNAs encoding human FAM48A were amplified from total RNA isolated from HeLa cells and subcloned into pIRESpuro4 (Clontech). pMXs-venus-mAtg9 was a kind gift from Dr. Masaaki Komatsu (Juntendo University School of Medicine, Tokyo, Japan). pMXs-mKate2-hRab11 was as previously described[33].

Cell culture and transfection

HEK293T, U2OS, and COS-1 cells were cultured under standard conditions. HBSS was used as a starvation medium. MG132 (Peptide Institute Inc.) and epoxomicin (UBPBio) were used for proteasome inhibition. COS-1 cells stably expressing Venus-mAtg9 and mKate2-hRab11 were established using retrovirus. Plat-E cells were transfected with pMXs-Venus-Atg9 or pMXs-mKate2-Rab11 together with pCMV-VSV-G-RSV-Rev (generously provided by Dr. Hiroyuki Miyoshi) using polyethyleneimine (PEI-MAX, MW 40,000; Polysciences). The medium containing the retrovirus was collected. COS-1 cells were incubated in the medium supplemented with 8 μg/ml polybrene (Sigma), followed by isolation of stably transfected cells using a cell sorter (SH800; Sony). FAM48A siRNAs were transfected into cells with RNAiMAX (Invitrogen). The sequences of the siRNAs are as follows: siFAM48A #1 (GGG AAA GAA ACA GAU CAA ACU GAA A) and siFAM48A #2 (GCU CUC CCA GUU UAC ACC ACA ACA A).

Antibodies and fluorescent reagents

The anti-α6 antibody was as described previously[88]. Anti-FAM48A antibody, anti-LC3 antibody, and anti-Atg9 antibody were kindly provided by Dr. Laszlo Tora (IGBMC, Strasbourg, France)[25], Dr. Masaaki Komatsu (Juntendo University School of Medicine, Tokyo, Japan)[89], and Dr. Yasuo Uchiyama (Juntendo University School of Medicine, Tokyo, Japan)[90], respectively. Anti-Flag M2 antibody, anti-GAPDH antibody (6C5), anti-LC3 antibody (PM036), anti-GM130 antibody, horseradish peroxidase-coupled secondary antibodies, and Alexa Fluor 488 (A11034 and A11029) and Alexa Fluor 647 (A21245 and A21236) were purchased from Sigma-Aldrich, Abcam, MBL, Jackson ImmunoResearch, and Invitrogen, respectively.

Immunoblotting

To detect LC3, cells were lysed with a buffer containing 50 mM Tris-HCl (pH 7.5), 1% (w/w) TritonX-100, 150 mM NaCl, 1 mM EDTA, and 1 mM PMSF. To detect proteins, cells were lysed in a buffer containing 50 mM Tris-HCl (pH 7.5) and 0.5% NP-40. Lysates were sonicated, cleared by centrifugation at 20,400 g for 10 min at 4°C, and boiled in a buffer containing 210 mM Tris-HCl (pH 6.8), 8.6% (w/w) sodium dodecyl sulfate (SDS), 28% (v/v) glycerol, 0.04% (w/w) bromophenol blue, and 20% (w/w) 2-mercaptoethanol. For subcellular fractionation, U2OS cells were homogenized with a Dounce homogenizer in a buffer containing 25 mM Tris-HCl (pH 7.5), 1 mM DTT, and 0.25 M sucrose and then centrifuged at 1,000 × g for 10 min at 4°C. The precipitates were dispersed in the same buffer and centrifuged at 1,000 × g for 10 min at 4°C. The

precipitates were used as the nuclear fraction, and the supernatants were used as the cytoplasmic fraction. Lysates were separated by SDS-PAGE, transferred onto a polyvinylidene difluoride membrane, and subjected to immunoblot analysis.

qPCR analysis

Total RNA was extracted using High Pure RNA Isolation Kit (Roche) and reverse-transcribed into cDNA with ReverTra Ace reverse transcriptase (Toyobo Co.). Probes were purchased from Roche Diagnostics. Real-time quantitative PCR was carried out on a LightCycler 480 (Roche) in triplicate. The ΔΔCt method was performed to calculate relative fold difference. The results are shown with the standard deviation (s.d.). The sequences of primers and probes used were as follows: FAM48A, 5′-TGT GGA TCT CAA TCA AGT TAG CA-3′ and 5′-AGC AGA GTT TGC CAT GAC CT-3′; with the Universal Probe Library (UPL) #78; LC3B, 5′-CGA ACC TTC GAA CAA AGA G-3′ and 5′-CTT CTC ACC CTT GTA TCG TTC TAT T -3′ with the UPL #89; and GUSB, 5′-CGC CCT GCC TAT CTG TAT TG-3′ and 5′-TCC CCA CAG GGA GTG TGT AG-3′ with the UPL #57.

Immunofluorescence microscopy

To detect LC3 puncta, cells were fixed with 4% perfluoroalkoxy alkane for 10 min, quenched with 50 mM NH_4Cl in PBS for 30 min, permeabilized with 50 μg/mL digitonin for 15 min, and blocked with PBS containing 5% bovine serum albumin, as previously described [91]. The ratio of the total area of LC3-positive puncta to the total

cellular area was quantified using Fiji[92]. To detect proteins other than LC3, cells were processed as previously described[93].

Flow cytometry analysis

Cells were suspended in PBS containing 1% FCS, 0.02% NaN_3, 2 mM EDTA, and 0.001% propidium iodide (Nacalai Tesque) and analyzed using Attune NxT (Life Technologies). Data were analyzed with FlowJo 10.

Materials and methods (Part B)

Mice

C57BL/6N mice and Lck Cre mice were purchased from Clea Japan and the Jackson Laboratory, respectively. Rpn11-GFP/+ KI reporter mice and Rpn13$^{flox/flox}$ mice were previously described[62,76]. All mice were maintained under specific pathogen-free conditions. All animal experiments were performed after obtaining approval from the Institutional Animal Care Committee of Graduate School of Pharmaceutical Sciences, the University of Tokyo (approval number M25-19).

RNA isolation and RNA sequencing

Total RNAs were isolated using the High Pure RNA Isolation Kit (Roche). RNA was used to prepare RNA-Seq libraries with a TruSeq RNA library preparation kit. The libraries were sequenced for 91 cycles (paired read) using a HiSeq 4000 sequencer (Illumina). Sequence reads from each cDNA library were mapped onto the mouse genome build mm9 using Tophat, and the mappable data were then processed by Cufflinks. The obtained data were normalized based on FPKM (fragments per kilobase exon model per million mapped reads). DEGs were detected with the PossionDis method based on the following parameters: fold change ≥2.00 and FDR ≤0.001. The genes for cell cycle signatures are listed in Supplementary Information.

RNA-Seq data were deposited in DNA Data Bank of Japan under accession number DRA008642.

Flow cytometry analysis

Flow cytometric analysis was performed with Attune NxT (Thermo Fisher Scientific), and data were analyzed with FlowJo software (Tree Star). Cells were subjected to Fc receptor blocking using anti-FcgR mAb (2.4G2) and stained with the following antibodies: anti-CD8α-FITC (BD Pharmingen), anti-CD45-PE-Cy7 (BD Pharmingen), anti-CD4-PE (BD Pharmingen), anti-CD3e-APC (BD Pharmingen), anti-CD44-PerCP-Cy5.5 (Biolegend), anti-CD62L-APC (BD Pharmingen), and anti-PD-1-APC-eFluor 780 antibodies (Invitrogen). Cells were suspended in staining buffer containing 0.5 mg/ml propidium iodide (Sigma) before analysis to exclude dead cells.

Cell isolation and cell sorting

Single-cell suspensions from the spleen were obtained by gently forcing the tissues through a nylon mesh grid in RPMI-1640 (Nacalai Tesque) containing 2% FBS (Hyclone). Splenic erythrocytes were eliminated with RBC lysis buffer (BioLegend). Cell sorting was performed with a FACSAria III or Cell sorter SH800. To sort $CD4^+$ T cell subsets, spleen cells were first depleted of $B220^+$, $CD8b^+$, and adherent cells by panning, and stained with PE-conjugated anti-mouse $CD4^+$ and other fluorescent antibodies as previously described[94]. These cells were subjected to cell sorting. The purity of sorted populations was invariably >95%.

Cell culture

Spleen cells or purified $CD4^+$ T cells were cultured in RPMI-1640 (Nacalai Tesque) supplemented with 10% FBS (Gibco), 10 mM HEPES (Nacalai Tesque), 50 μM 2-ME (Sigma-Aldrich), 100 U/ml penicillin and 100 μg/ml streptomycin (Nacalai Tesque), and 2.5 ng/mL IL-2 (BioLegend). For *in vitro* T cell activation, splenocytes or $CD4^+$ T cells were cultured with immobilized anti-CD3e mAb (0.5 μg/mL, 145-2C11, BioLegend) for two days.

Immunoblot analysis

Cells were lysed in a buffer containing 25 mM Tris-HCl (pH 7.5), 1 mM dithiothreitol (DTT), 2 mM ATP, 5 mM $MgCl_2$, and 0.2% NP-40. Extracted proteins were boiled with 4× SDS loading buffer, electrophoresed in a polyacrylamide gel, and transferred to polyvinylidene difluoride membranes. Membranes were soaked in Blocking One (Nacalai Tesque) and immunoreacted with the primary antibodies and secondary antibodies conjugated to horseradish peroxidase (Jackson ImmunoResearch, dilution 1:20,000). Images were cropped for presentation. Protein bands were visualized by incubation with Western Lightning Plus-ECL reagent (Perkin Elmer), and images were acquired using ImageQuant LAS 4000mini (GE Healthcare).

Glycerol gradient analysis and proteasome activity assay

Cell lysates were clarified by centrifugation at 20,000 *g*, and subjected to 8–32% (vol/vol) linear glycerol gradient centrifugation (22 h, 83,000 *g*) as described previously[95].

Peptidase activity was measured using a fluorescent peptide substrate, Suc-LLVY-MCA and Z-LLE-MCA, as described previously[95].

ChIP-Seq data analysis

Analysis of binding proteins at proteasome gene loci was performed by in silico ChIP analysis in ChIP-Atlas[72]. The following genes of constitutively expressed proteasome subunits were used for *in silico* ChIP analysis: PSMA1, PSMA2, PSMA3, PSMA4, PSMA5, PSMA6, PSMA7, PSMB1, PSMB2, PSMB3, PSMB4, PSMB5, PSMB6, PSMB7, PSMC1, PSMC2, PSMC3, PSMC4, PSMC5, PSMC6, PSMD1, PSMD2, PSMD3, PSMD4, PSMD6, PSMD7, PSMD8, PSMD11, PSMD12, PSMD13, PSMD14, ADRM1, and SEM1.

Analysis of the ChIP-Seq data shown in Fig. 9b was performed using raw data from the NCBI database (GEO GSE39756)[74].

Statistical analysis

Statistical analysis was performed using the Student's t-test or Tukey's test.

Reference

1. Coux, O., Tanaka, K. & Goldberg, A. L. Structure and functions of the 20S and 26S proteasomes. *Annu. Rev. Biochem.* **65,** 801–847 (1996).
2. Avram, Hershko; Aaron, C. The ubiquitin system. *Annu. Rev. Biochem.* **67,** 425–479 (1998).
3. Mizushima, N. & Komatsu, M. Autophagy: Renovation of cells and tissues. *Cell* **147,** 728–741 (2011).
4. Yan, J. *et al.* Overexpression of Human E46K Mutant α-Synuclein Impairs Macroautophagy via Inactivation of JNK1-Bcl-2 Pathway. *Mol. Neurobiol.* **50,** 685–701 (2014).
5. Winslow, A. R. *et al.* α-Synuclein impairs macroautophagy: implications for Parkinson's disease. *J. Cell Biol.* **190,** 1023–1037 (2010).
6. Tanik, S. A., Schultheiss, C. E., Volpicelli-Daley, L. A., Brunden, K. R. & Lee, V. M. Y. Lewy Body-like α-Synuclein Aggregates Resist Degradation and Impair Macroautophagy. *J. Biol. Chem.* **288,** 15194–15210 (2013).
7. Song, J. *et al.* HMGB1 is involved in autophagy inhibition caused by SNCA/α-synuclein overexpression. *Autophagy* **10,** 144–154 (2014).
8. Wang, K. *et al.* Beclin1 and HMGB1 ameliorate the α -synuclein-mediated autophagy inhibition in PC12 cells. *Diagn. Pathol.* 1–10 (2016). doi:10.1186/s13000-016-0459-5

9. Tseng, B. P., Green, K. N., Chan, J. L., Blurton-Jones, M. & LaFerla, F. M. Aβ inhibits the proteasome and enhances amyloid and tau accumulation. *Neurobiol. Aging* **29,** 1607–1618 (2008).

10. Bence, N. F., Sampat, R. M. & Kopito, R. R. Impairment of the ubiquitin-proteasome system by protein aggregation. *Science (80-.).* **292,** 1552–5 (2001).

11. Koizumi, S. *et al.* The aspartyl protease DDI2 activates Nrf1 to compensate for proteasome dysfunction. *Elife* **5,** 1–10 (2016).

12. Radhakrishnan, S. K. *et al.* Transcription factor Nrf1 mediates the proteasome recovery pathway after proteasome inhibition in mammalian cells. *Mol. Cell* **38,** 17–28 (2010).

13. Steffen, J., Seeger, M., Koch, A. & Krüger, E. Proteasomal degradation is transcriptionally controlled by TCF11 via an ERAD-dependent feedback loop. *Mol. Cell* **40,** 147–158 (2010).

14. Pandey, U. B. *et al.* HDAC6 rescues neurodegeneration and provides an essential link between autophagy and the UPS. *Nature* **447,** 860–864 (2007).

15. Jiang, S. *et al.* Participation of proteasome-ubiquitin protein degradation in autophagy and the activation of AMP-activated protein kinase. *Cell. Signal.* **27,** 1186–1197 (2015).

16. Min, H. *et al.* Bortezomib induces protective autophagy through AMP-activated protein kinase activation in cultured pancreatic and colorectal cancer cells. *Cancer Chemother. Pharmacol.* **74,** 167–176 (2014).

17. Sun, A. *et al.* GSK-3β controls autophagy by modulating LKB1-AMPK pathway in prostate cancer cells. *Prostate* **76,** 172–183 (2016).

18. Senft, D. & Ronai, Z. A. crosstalk underlies the ER stress response. *Trends Biochem. Sci.* **40,** 141–148 (2015).

19. Brüning, A., Rahmeh, M. & Friese, K. Nelfinavir and bortezomib inhibit mTOR activity via ATF4-mediated sestrin-2 regulation. *Mol. Oncol.* **7,** 1012–1018 (2013).

20. Høyer-Hansen, M. & Jäättelä, M. Connecting endoplasmic reticulum stress to autophagy by unfolded protein response and calcium. *Cell Death Differ.* **14,** 1576–1582 (2007).

21. Natsume, T. *et al.* A Direct Nanoflow Liquid Chromatography−Tandem Mass Spectrometry System for Interaction Proteomics. *Anal. Chem.* **74,** 4725–4733 (2002).

22. Webber, J. L. & Tooze, S. A. Coordinated regulation of autophagy by p38a MAPK through mAtg9 and p38IP. *EMBO J.* **29,** 27–40 (2010).

23. Liu, X. *et al.* The p38-Interacting protein (p38IP) regulates G2/M progression by promoting α-Tubulin acetylation via inhibiting ubiquitination-Induced degradation of the acetyltransferase GCN5. *J. Biol. Chem.* **288,** 36648–36661 (2013).

24. Zohn, I. E. *et al.* p38 and a p38-Interacting Protein Are Critical for Downregulation of E-Cadherin during Mouse Gastrulation. *Cell* **125,** 957–969 (2006).

25. Nagy, Z. *et al.* The Human SPT20-Containing SAGA Complex Plays a Direct Role in the Regulation of Endoplasmic Reticulum Stress-Induced Genes. *Mol. Cell. Biol.* **29,** 1649–1660 (2009).

26. Dikic, I. Proteasomal and Autophagic Degradation Systems. *Annu. Rev. Biochem.* **86,** 193–224 (2017).

27. Mizushima, N., Yoshimori, T. & Levine, B. Methods in Mammalian Autophagy Research. *Cell* **140,** 313–326 (2010).

28. Milani, M. *et al.* The role of ATF4 stabilization and autophagy in resistance of breast cancer cells treated with Bortezomib. *Cancer Res.* **69,** 4415–4423 (2009).

29. Young, A. R. J. Starvation and ULK1-dependent cycling of mammalian Atg9 between the TGN and endosomes. *J. Cell Sci.* **119,** 3888–3900 (2006).

30. Longatti, A. *et al.* TBC1D14 regulates autophagosome formation via Rab11- and ULK1-positive recycling endosomes. *J. Cell Biol.* **197,** 659–675 (2012).

31. Popovic, D. & Dikic, I. TBC1D5 and the AP2 complex regulate ATG9 trafficking and initiation of autophagy. *EMBO Rep.* **15,** 392–401 (2014).

32. Puri, C., Renna, M., Bento, C. F., Moreau, K. & Rubinsztein, D. C. Diverse autophagosome membrane sources coalesce in recycling endosomes. *Cell* **154,** 1285–1299 (2013).

33. Misaki, R., Nakagawa, T., Fukuda, M., Taniguchi, N. & Taguchi, T. Spatial segregation of degradation- and recycling-trafficking pathways in COS-1 cells. *Biochem. Biophys. Res. Commun.* **360,** 580–585 (2007).

34. Orsi, A. *et al.* Dynamic and transient interactions of Atg9 with autophagosomes, but not membrane integration, are required for autophagy. *Mol. Biol. Cell* **23,** 1860–1873 (2012).

35. Imai, K. *et al.* Atg9A trafficking through the recycling endosomes is required for autophagosome formation. *J. Cell Sci.* **129,** 3781–3791 (2016).

36. Osawa, T. *et al.* Atg2 mediates direct lipid transfer between membranes for autophagosome formation. *Nat. Struct. Mol. Biol.* **26,** 281–288 (2019).

37. Gómez-Sánchez, R. *et al.* Atg9 establishes Atg2-dependent contact sites between the endoplasmic reticulum and phagophores. *J. Cell Biol.* **217,** 2743–2763 (2018).

38. Knævelsrud, H. *et al.* Membrane remodeling by the PX-BAR protein SNX18 promotes autophagosome formation. *J. Cell Biol.* **202,** 331–349 (2013).

39. Adams, J. The development of proteasome inhibitors as anticancer drugs. *Cancer Cell* **5,** 417–421 (2004).

40. Vilchez, D. *et al.* Increased proteasome activity in human embryonic stem cells is regulated by PSMD11. *Nature* **489,** 304–308 (2012).

41. Zhang, Y. *et al.* Coordinated regulation of protein synthesis and degradation by mTORC1. *Nature* **513,** 440–443 (2014).

42. Vilchez, D. *et al.* RPN-6 determines C. elegans longevity under proteotoxic stress conditions. *Nature* **489,** 263–268 (2012).

43. Rodriguez, K. A., Edrey, Y. H., Osmulski, P., Gaczynska, M. & Buffenstein, R. Altered composition of liver proteasome assemblies contributes to enhanced

proteasome activity in the exceptionally long-lived naked mole-rat. *PLoS One* **7,** (2012).

44. Tonoki, A. *et al.* Genetic evidence linking age-dependent attenuation of the 26S proteasome with the aging process. *Mol. Cell. Biol.* **29,** 1095–1106 (2009).

45. Sasaki, K. *et al.* PAC1 gene knockout reveals an essential role of chaperone-mediated 20S proteasome biogenesis and latent 20S proteasomes in cellular homeostasis. *Mol. Cell. Biol.* **30,** 3864–74 (2010).

46. Tomaru, U. *et al.* Decreased proteasomal activity causes age-related phenotypes and promotes the development of metabolic abnormalities. *Am. J. Pathol.* **180,** 963–972 (2012).

47. Torres, C., Lewis, L. & Cristofalo, V. J. Proteasome inhibitors shorten replicative life span and induce a senescent-like phenotype of human fibroblasts. *J. Cell. Physiol.* **207,** 845–853 (2006).

48. Brehm, A. & Krüger, E. Dysfunction in protein clearance by the proteasome: Impact on autoinflammatory diseases. *Semin. Immunopathol.* **37,** 323–333 (2015).

49. Brehm, A. *et al.* Additive loss-of-function proteasome subunit mutations in CANDLE/PRAAS patients promote type I IFN production. *J. Clin. Invest.* **125,** 4196–4211 (2015).

50. Arima, K. *et al.* Proteasome assembly defect due to a proteasome subunit beta type 8 (PSMB8) mutation causes the autoinflammatory disorder, Nakajo-Nishimura syndrome. *Proc. Natl. Acad. Sci.* **108,** 14914–14919 (2011).

51. McDermott, A., Jacks, J., Kessler, M., Emanuel, P. D. & Gao, L. Proteasome-associated autoinflammatory syndromes: advances in pathogeneses, clinical presentations, diagnosis, and management. *Int. J. Dermatol.* **54,** 121–129 (2015).

52. Linton, P. J. & Dorshkind, K. Age-related changes in lymphocyte development and function. *Nat. Immunol.* **5,** 133–139 (2004).

53. Cavanagh, M. M., Weyand, C. M. & Goronzy, J. J. Chronic inflammation and aging: DNA damage tips the balance. *Curr. Opin. Immunol.* **24,** 488–493 (2012).

54. Maue, A. C. *et al.* T-cell immunosenescence: lessons learned from mouse models of aging. *Trends Immunol.* **30,** 301–305 (2009).

55. Haynes, L. & Swain, S. L. Aged-related shifts in T cell homeostasis lead to intrinsic T cell defects. *Semin. Immunol.* **24,** 350–355 (2012).

56. Shimatani, K., Nakashima, Y., Hattori, M., Hamazaki, Y. & Minato, N. PD-1+ memory phenotype CD4+ T cells expressing C/EBPalpha underlie T cell immunodepression in senescence and leukemia. *Proc. Natl. Acad. Sci. U. S. A.* **106,** 15807–12 (2009).

57. Berges, C. *et al.* Proteasome inhibition suppresses essential immune functions of human CD4 + T cells. *Immunology* **124,** 234–246 (2008).

58. Yanaba, K. *et al.* The proteasome inhibitor bortezomib inhibits T cell-dependent inflammatory responses. *J. Leukoc. Biol.* **88,** 117–122 (2010).

59. Saez, I. & Vilchez, D. The mechanistic links between proteasome activity, aging and age-related diseases. *Curr. Genomics* **15,** 38–51 (2014).

60. Kuilman, T., Michaloglou, C., Mooi, W. J. & Peeper, D. S. The essence of senescence. *Genes Dev.* **24,** 2463–2479 (2010).

61. Mizuno, H., Nakanishi, Y., Ishii, N., Sarai, A. & Kitada, K. A signature-based method for indexing cell cycle phase distribution from microarray profiles. *BMC Genomics* **10,** 137 (2009).

62. Hamazaki, J., Hirayama, S. & Murata, S. Redundant roles of Rpn10 and Rpn13 in recognition of ubiquitinated proteins and cellular homeostasis. *PLOS Genet.* **11,** e1005401 (2015).

63. Shi, J. & Petrie, H. T. Activation kinetics and off-target effects of thymus-initiated Cre transgenes. *PLoS One* **7,** e46590 (2012).

64. Carow, B., Gao, Y., Coquet, J., Reilly, M. & Rottenberg, M. E. lck-Driven Cre expression alters T cell development in the thymus and the frequencies and functions of peripheral T cell subsets. *J. Immunol.* **197,** 2261–2268 (2016).

65. Huang, D. W., Sherman, B. T. & Lempicki, R. A. Bioinformatics enrichment tools: Paths toward the comprehensive functional analysis of large gene lists. *Nucleic Acids Res.* **37,** 1–13 (2009).

66. Baumeister, W., Walz, J., Zühl, F. & Seemüller, E. The proteasome: Paradigm of a self-compartmentalizing protease. *Cell* **92,** 367–380 (1998).

67. Kaneko, T. *et al.* Assembly pathway of the mammalian proteasome base subcomplex is mediated by multiple specific chaperones. *Cell* **137,** 914–925 (2009).

68. Ramos, P. C. & Dohmen, R. J. PACemakers of proteasome core particle assembly. *Structure* **16,** 1296–1304 (2008).

69. Kusmierczyk, A. R., Kunjappu, M. J., Funakoshi, M. & Hochstrasser, M. A multimeric assembly factor controls the formation of alternative 20S proteasomes. *Nat. Struct. Mol. Biol.* **15,** 237–244 (2008).

70. Murata, S., Yashiroda, H. & Tanaka, K. Molecular mechanisms of proteasome assembly. *Nat. Rev. Mol. Cell Biol.* **10,** 104–115 (2009).

71. Kalim, K. W., Basler, M., Kirk, C. J. & Groettrup, M. Immunoproteasome Subunit LMP7 Deficiency and Inhibition Suppresses Th1 and Th17 but Enhances Regulatory T Cell Differentiation. *J. Immunol.* **189,** 4182–4193 (2012).

72. Oki, S. *et al.* Integrative analysis of transcription factor occupancy at enhancers and disease risk loci in noncoding genomic regions. *bioRxiv* (2018). doi:https://doi.org/10.1101/262899

73. Kappelmann, M., Bosserhoff, A. & Kuphal, S. AP-1/c-Jun transcription factors: Regulation and function in malignant melanoma. *Eur. J. Cell Biol.* **93,** 76–81 (2014).

74. Li, P. *et al.* BATF-JUN is critical for IRF4-mediated transcription in T cells. *Nature* **490,** 543–546 (2012).

75. Gorentla, B. K. & Zhong, X.-P. T cell receptor signal transduction in T lymphocytes. *J. Clin. Cell. Immunol.* **2012,** 5 (2012).

76. Tomita, T. *et al.* Specific modification of aged proteasomes revealed by tag-exchangeable knock-in mice. *Mol. Cell. Biol.* **39,** (2018).

77. Motosugi, R. & Murata, S. Dynamic regulation of proteasome expression. *Front. Mol. Biosci.* **6,** 4–11 (2019).

78. Lee, S. *et al.* Involvement of the Nrf2-proteasome pathway in the endoplasmic reticulum stress response in pancreatic β -cells. *Toxicol. Appl. Pharmacol.* **264,** 431–438 (2012).

79. Pickering, A. M., Linder, R. A., Zhang, H., Forman, H. J. & Davies, K. J. A. Nrf2-dependent induction of proteasome and Pa28αβ regulator are required for adaptation to oxidative stress. *J. Biol. Chem.* **287,** 10021–10031 (2012).

80. Vangala, J. R., Dudem, S., Jain, N. & Kalivendi, S. V. Regulation of PSMB5 protein and β subunits of mammalian proteasome by constitutively activated signal transducer and activator of transcription 3 (STAT3). *J. Biol. Chem.* **289,** 12612–12622 (2014).

81. Lu, L. *et al.* Ameliorating replicative senescence of human bone marrow stromal cells by PSMB5 overexpression. *Biochem. Biophys. Res. Commun.* **443,** 1182–1188 (2014).

82. Shin, S.-W. *et al.* Mouse zygote-specific proteasome assembly chaperone important for maternal-to-zygotic transition. *Biol. Open* **2,** 170–182 (2013).

83. Tahir, S. *et al.* A CD153+ CD4+ T follicular cell population with cell-senescence features plays a crucial role in lupus pathogenesis via osteopontin production. *J. Immunol.* **194,** 5725–5735 (2015).

84. Xu, H. *et al.* The CCAAT box-binding transcription factor NF-Y regulates basal expression of human proteasome genes. *Biochim. Biophys. Acta - Mol. Cell Res.* **1823,** 818–825 (2012).

85. Pahlavani, M. A. & Vargas, D. M. Age-related decline in activation of calcium/calmodulin-dependent phosphatase calcineurin and kinase CaMK-IV in rat T cells. *Mech. Ageing Dev.* **112,** 59–74 (1999).

86. Trebilcock, G. U. & Ponnappan, U. Nuclear factor-κB induction in CD45RO+ and CD45RA+ T cell subsets during aging. *Mech. Ageing Dev.* **102,** 149–163 (1998).

87. Shirakawa, K. *et al.* Obesity accelerates T cell senescence in murine visceral adipose tissue. **126,** (2016).

88. Tanashi, N., Murakami, Y. & Minami, Y. Hybrid proteasomes. *J. Biol. Chem* **275,** 14336–14345 (2000).

89. Komatsu, M. *et al.* Homeostatic Levels of p62 Control Cytoplasmic Inclusion Body Formation in Autophagy-Deficient Mice. *Cell* **131,** 1149–1163 (2007).

90. Tamura, H., Shibata, M., Koike, M., Sasaki, M. & Uchiyama, Y. Atg9A protein, an autophagy-related membrane protein, is localized in the neurons of mouse brains. *J. Histochem. Cytochem.* **58,** 443–453 (2010).

91. Kageyama, S. *et al.* The LC3 recruitment mechanism is separate from Atg9L1-dependent membrane formation in the autophagic response against Salmonella. *Mol. Biol. Cell* **22,** 2290–2300 (2011).

92. Schindelin, J. *et al.* Fiji: An open-source platform for biological-image analysis. *Nat. Methods* **9,** 676–682 (2012).

93. Hirayama, S. *et al.* Nuclear export of ubiquitinated proteins via the UBIN-POST system. *Proc. Natl. Acad. Sci.* 201711017 (2018). doi:10.1073/pnas.1711017115

94. Hayatsu, N. *et al.* Analyses of a mutant Foxp3 allele reveal BATF as a critical transcription factor in the differentiation and accumulation of tissue regulatory T cells. *Immunity* **47,** 268–283.e9 (2017).

95. Hirano, Y. *et al.* A heterodimeric complex that promotes the assembly of mammalian 20S proteasomes. *Nature* **437,** 1381–1385 (2005).

謝辞

本研究を行うにあたりご指導頂いた村田茂穂教授、蛋白質代謝学教室のスタッフの先生方、並びに学生の皆様に厚く御礼申し上げます。特に村田先生、八代田先生、濱崎先生には 4 年生で教室配属になり、足掛け 10 年以上に渡りお世話になり、感謝の思いでいっぱいです。

また、本研究内容を進めるにあたりご協力頂いた、とりわけ以下の共著者の皆様に感謝申し上げます。

“FAM48A mediates compensatory autophagy induced by proteasome impairment”については、渡邊綾香さん、本杉良さん、家村俊一郎教授、夏目徹創薬分子プロファイリング研究センター長、向井康治朗助教、田口友彦教授、平山尚志郎助教、濱崎純助教、村田茂穂教授

“Defective induction of the proteasome associated with T cell receptor signaling underlies T cell senescence”については渡邊綾香さん、本杉良さん、村上龍一助教、後藤剛志さん、堀昌平教授、平山尚志郎助教、濱崎純助教、村田茂穂教授

最後に研究生活を支えてくれた家族に感謝申し上げます。